

**Using Dynamic Thermal Rating of HVDC Transmission Corridors  
to Increase Penetration of Renewable Energy**

by

Beddage Veenavi Wasundara Pemachandra

A thesis submitted in partial fulfillment of the requirements for the degree of

Master of Science

in

Energy Systems

Department of Electrical and Computer Engineering  
University of Alberta

© Beddage Veenavi Wasundara Pemachandra, 2024

# Abstract

As the world shifts its focus toward achieving net-zero emissions, every contributor to greenhouse gas emissions, including the electricity industry, is transitioning to eco-friendly solutions such as renewable generation. Simultaneously, the significant increase in electrical consumption has also highlighted the need to increase the capacity of the transmission infrastructure. As a result, much attention has been paid to the large-scale use of renewable energy through high-voltage direct current (HVDC) transmission technology, ascribing to its economic feasibility. The growing demand for electricity and the increasing penetration of renewable energy sources has prompted the electric power industry to explore methods to optimize the use of existing grid infrastructure.

Dynamic Thermal Line Rating (DTLR) is one of the promising techniques that allow transmission lines to operate close to their actual maximum capacity considering real-time operating conditions such as conductor temperature, sag, tension, and weather parameters. Numerous practical implementations and studies on this subject have been carried out thus far starting from the period before World War 2. However, the majority of existing research on this topic has been limited to employing DTLR in classical alternating current based power systems.

To this end, this study presents a novel approach by employing DTLR for an HVDC transmission system to maximize the utilization of the transmission capacity and to improve the penetration of renewable energy. This approach can allow the transmission utility companies to expand their utilization of renewable energy integration to the generation mix while reducing or even avoiding capital investments

into new transmission line infrastructure.

The feasibility and performance of the proposed approach are evaluated by conducting a case study for an HVDC transmission line in Alberta, Canada. The study results find that, on average, the mean increase in HVDC line conductor ampacity rating above the static rating is 64% during winter and 34% during summer. This additional capacity is proposed to integrate wind energy, replacing coal-fired energy generation. This would lead to a significant reduction in greenhouse gas emissions, especially a 13.78 tons per hour reduction in carbon dioxide ( $CO_2$ ). Furthermore, the financial benefits comparison indicates an additional benefit of CA\$ 0.10 M/GWh when using DTLR for enhancing the transmission capacity rather than the conventional line upgrading method. Ultimately, this study offers a practical approach to reducing greenhouse gas emissions by integrating more renewable energy resources into the generation mix and reducing curtailment. Furthermore, looking into the global scale, since the long distance transmission from HVDC is gaining more popularity, this will allow the utility companies to optimally choose the best locations where renewable sources are available even though they are either offshore or far away from the load centers.

# Preface

This thesis research is an original work by Beddage Veenavi Wasundara Pemachandra. A dynamic thermal line rating technique is employed to optimize HVDC transmission corridors while enhancing renewable generation and reducing greenhouse gas emissions.

Parts of Chapter 3, Chapter 4, and Chapter 6 of this thesis have been submitted for consideration for publication as Veenavi Pemachandra, Petr Musilek, Gregory Kish, "Optimizing HVDC Transmission Corridors: Dynamic Thermal Line Rating for Enhanced Renewable Generation and GHG Emission Reduction". © MDPI Energies (Under review).

In this thesis, I was responsible for conceptualization, data collection, data analysis, python programming, and writing. Dr. Petr Musilek and Dr. Gregory Kish were my academic supervisors, who provided me with resources and were involved with conceptualization, methodology, supervision, validation, analysis, review, and editing.

# Acknowledgements

I would like to extend my sincere gratitude to all those who supported me throughout these two years of my graduate studies at the University of Alberta to the completion of my master's degree. First and foremost I would like to thank my supervisors Dr. Petr Musilek and Dr. Gregory Kish for believing in me and giving me this valuable opportunity. Your guidance, support, and invaluable insights throughout this journey have always been the encouragement for me to shape the direction of my work.

I am also thankful to the members of the examination committee for their time and all the valuable comments, and recommendations on enriching the quality of this work.

I would extend my thanks to the University of Alberta and the Department of Electrical and Computer Engineering for facilitating the necessary resources for undertaking this research.

I am grateful to my colleagues and peers in my two research groups; ENTAIL and PEPST Lab for helping me whenever needed and giving me valuable ideas.

I want to express my heartfelt appreciation to my parents, and my brother for supporting me in taking this opportunity and pushing me toward higher studies. Their encouragement and endless support were the biggest pillars behind my success. Last but not least, I would like to thank my husband, for his support, love, encouragement, patience, and for always being there for me.

# Table of Contents

<b>1</b>	<b>Introduction</b>	<b>1</b>
1.1	Motivation . . . . .	1
1.2	Thesis Objectives . . . . .	2
1.3	Thesis Outline . . . . .	3
<b>2</b>	<b>Literature Review</b>	<b>5</b>
2.1	Dynamic Thermal Line Rating (DTLR) Technology Overview . . . . .	5
2.2	Previous studies on DTLR . . . . .	6
2.3	Applications of DTLR in Wind Power Integration . . . . .	9
2.4	HVDC systems overview . . . . .	12
2.4.1	History of HVDC . . . . .	12
2.4.2	HVDC Converter Technologies . . . . .	13
2.4.3	HVDC Link Configurations . . . . .	15
2.5	Role of HVDC in Renewable Energy Integration . . . . .	18
2.6	Key outcomes of the literature review . . . . .	20
<b>3</b>	<b>Methodological Framework for DTLR Calculation and Wind Energy Assessment</b>	<b>22</b>
3.1	Conductor Rating and Ampacity . . . . .	22
3.2	Overview of relevant technical standards . . . . .	23
3.3	Heat Balance Equation . . . . .	25
3.3.1	Convective heat loss ( $q_c$ ) . . . . .	26

3.3.2	Radiated heat loss ( $q_r$ ) . . . . .	28
3.3.3	Solar heat gain ( $q_s$ ) . . . . .	28
3.3.4	Joule heat gain ( $q_j$ ) . . . . .	29
3.4	Wind Energy . . . . .	30
3.5	GHG Emissions From Electric Sector . . . . .	33
<b>4</b>	<b>Dynamic Thermal Line Rating &amp; Wind Power Generation</b>	<b>35</b>
4.1	HVDC system case study for DTLR analysis . . . . .	35
4.1.1	Study system . . . . .	36
4.1.2	Meteorological data collection . . . . .	38
4.1.3	Overall methodology followed for DTLR calculations and wind energy assessment . . . . .	39
4.2	Results . . . . .	41
4.2.1	Dynamic thermal line rating calculation . . . . .	41
4.2.2	Wind Power Generation . . . . .	45
4.2.3	GHG Reduction . . . . .	46
4.3	Discussion . . . . .	47
<b>5</b>	<b>Economic Analysis</b>	<b>50</b>
5.1	Introduction . . . . .	50
5.2	Scenario (1): Applying DTLR to the existing transmission line . . . . .	51
5.3	Scenario (2): Upgrading transmission line conductor size . . . . .	55
5.4	Financial benefit comparison . . . . .	57
<b>6</b>	<b>Conclusions &amp; Future Work</b>	<b>59</b>
6.1	Conclusions . . . . .	59
6.2	Future Work . . . . .	61
	<b>Bibliography</b>	<b>62</b>

# List of Tables

2.1	Previous studies and pilot projects on DTLR . . . . .	7
2.2	LCC-HVDC projects for renewable energy integration in China [77] .	20
3.1	Average GHG emission over life cycle by each generation technology. [89] . . . . .	33
3.2	Key pollutants discharged by coal power plants. [89] . . . . .	34
4.1	Assumed HVDC line conductor parameters . . . . .	38
4.2	Jenner wind farm specifications . . . . .	38
4.3	GHG emission reduction by JWPP2 wind plant by using DTLR . . .	46
5.1	Encor’s electricity price history in Alberta from 2021-11-01 to 2022-10-31	54
5.2	Financial benefit comparison . . . . .	57
5.3	Qualitative benefit comparison . . . . .	58

# List of Figures

2.1	Simple representation of an HVDC link [51] . . . . .	14
2.2	Monopolar link with a) Metallic return b) ground return [58] . . . . .	16
2.3	Bipolar link with ground return [58] . . . . .	17
2.4	Bipolar link with metallic return [58] . . . . .	17
2.5	Back-to-Back configuration[58] . . . . .	18
2.6	Homopolar Configuration[58] . . . . .	18
3.1	Heat balance of an overhead conductor . . . . .	25
3.2	Transmission line divided into sections . . . . .	30
3.3	General representation of a wind turbine power curve [91] . . . . .	31
4.1	Study system configuration . . . . .	36
4.2	Location map of EATL and Jenner wind farms . . . . .	37
4.3	Power curve for Enercon E-147 5MW turbine [103] . . . . .	39
4.4	Overall methodology . . . . .	40
4.4	DTLR variation of the line for six winter months (2021-11-01 to 2022-04-31) . . . . .	42
4.5	DTLR variation of the line for six summer months (2022-05-01 to 2022-10-31) . . . . .	43
4.6	Hourly average DTLR variation of a day . . . . .	44
4.7	Power generated by a single turbine at JWPP2 in January . . . . .	45
4.8	Average turbine output variation at JWPP2 for a day . . . . .	46

# List of Symbols

$\alpha$	Solar absorptivity
$\beta$	Pitch angle
$\epsilon$	Emissivity
$\lambda_i$	Tip speed ratio
$\mu_f$	Dynamic viscosity of air (kg/m-s)
$\phi$	Angle between wind and axis of conductor (deg)
$\rho_f$	Density of air ( $kg/m^3$ )
$\theta$	Effective angle of incidence of the sun's rays (deg)
$A'$	Projected area of conductor ( $m^2$ )
$C_p$	Coefficient of performance
$D_o$	Outside diameter of conductor (m)
$H_c$	Altitude of sun (0 to 90 deg)
$h_e$	Elevation of conductor above sea level (m)
$I$	Conductor current (A)
$K_f$	Thermal conductivity of air at temperature $T_{film}$ (W/(m-°C))
$K_{angle}$	Wind direction factor
$N_{re}$	Dimensionless Reynolds number
$q_c$	convective heat loss (W/m)

$q_i$	Corona heating (W/m)
$q_j$	Joule heating (W/m)
$q_m$	Magnetic heating (W/m)
$q_r$	Radiated heat loss (W/m)
$q_s$	Solar heat gain (W/m)
$q_w$	Evaporative cooling (W/m)
$q_{c1}$	Forced convection loss at lower wind speeds (W/m)
$q_{c2}$	Forced convection loss at higher wind speeds (W/m)
$q_{cn}$	Natural Convection (W/m)
$Q_{se}$	Total solar and sky radiated heat intensity corrected for elevation ( $W/m^2$ )
$R_{T_{avg}}$	AC resistance of conductor at temperature, $T_{avg}$ ( $\omega/m$ )
$R_{T_{high}}$	AC resistance at high average conductor temperature $T_{high}$ ( $\omega/m$ )
$R_{T_{low}}$	AC resistance at low average conductor temperature $T_{low}$ ( $\omega/m$ )
$T_a$	Ambient air temperature ( $^{\circ}C$ )
$T_s$	Conductor surface temperature ( $^{\circ}C$ )
$T_{film}$	Average temperature of the boundary layer $(T_s + T_a)/2$ ( $^{\circ}C$ )
$v_w$	Wind velocity (m/s)
$Z_1$	Azimuth of line (deg)
$Z_c$	Azimuth of sun (deg)

# Abbreviations

**AC** Alternating Current.

**ACIS** Alberta Climate Information Service.

**ACSR** Aluminium Conductor Steel-Reinforced.

**AESO** Alberta Electric System Operator.

**ANM** Active Network Management.

**CAD** Canadian Dollars.

**CCC** Current Carrying Capacity.

**CIGRE** International Council on Large Electric Systems.

**CSC** Current Source Converter.

**DC** Direct Current.

**DTLR** Dynamic Thermal Line Rating.

**EATL** Eastern Alberta Transmission Line.

**GHG** Greenhouse Gas.

**HVAC** High-Voltage Alternating Current.

**HVDC** High-Voltage Direct Current.

**IEEE** Institute of Electrical and Electronics Engineers.

**IGBT** Insulated Gate Bipolar Transistor.

**JWPP** Jenner Wind Power Project.

**LCC** Line-Commutated Converter.

**SR** Static Rating.

**TSO** Transmission System Operator.

**VSC** Voltage Source Converter.

**WATL** Western Alberta Transmission Line.

# Chapter 1

## Introduction

### 1.1 Motivation

Recent economic growth has resulted in a significant increase in electrical consumption, driving an increase in the demand for electrical power [1, 2]. To meet the growing demand, utilities are opting to boost renewable generation in their energy mix instead of relying on traditional sources like coal-fired plants [3]. This will require additional capacities in all parts of the electrical system, including generation, transmission, and distribution. However, the addition of new infrastructure not only increases costs but also the construction time [4]. As a result, electrical utility companies, government organizations, and professional bodies are actively exploring technologies to optimally utilize the existing power system infrastructure [5].

One of the main components that limit the power transfer capability in an electrical network is the rating of the transmission lines [2]. The rating of a conductor is usually defined considering the maximum allowable temperature of the conductor [6]. The current rating considered by the electrical utility companies, which is known as the “nominal rating” or “static rating (SR)”, is calculated by considering worst-case weather conditions, which are often very conservative [7]. It should also be noted that the simultaneous occurrence of these conditions is unlikely in real-world scenarios [2]. Consequently, the SR of overhead lines is usually much lower than the actual allowable current carrying capacity of the line [8].

Dynamic thermal line rating (DTLR) is a technique that allows transmission lines to operate much closer to their maximum capacity, considering their real-time operating conditions [6, 9]. Due to its many advantages, including moving more power using existing transmission corridors while maintaining a safe operating environment, DTLR has recently been employed in many transmission and distribution applications and has also been an important topic of research [2, 10–13].

However, to date, the DTLR concept has been predominantly applied in alternative current (AC) systems, and its presence in direct current (DC) applications is limited [14]. Interestingly, the CIGRE WG B2.43 [15] standard explicitly highlights the applicability of thermal rating calculations for both AC and DC operation, particularly in high-temperature and high-current density scenarios. Concurrently and unrelatedly, much attention has been paid to the collection and transmission of large-scale renewable energy through high-voltage direct current (HVDC) transmission corridors. Ascribing to its economic feasibility, this opens up the possibility of extending the use of the DTLR concept to HVDC systems. By identifying the opportunity to apply DTLR in HVDC systems for seamless renewable integration, this study aims to bridge this knowledge gap.

## 1.2 Thesis Objectives

The primary objective of this thesis is to maximize the capacity utilization of HVDC transmission corridors and facilitate the increased integration of renewable energy by utilizing DTLR. To achieve the primary objective, a case study is designed to apply the DTLR concept to a 500 kV HVDC transmission line in Alberta, Canada. Under the primary objective, the following sub-objectives were defined.

1. Identify and collect necessary data (meteorological data) for the study and conduct the calculations according to the selected standard to interpret the DTLR values of the considered HVDC transmission line to assess the excess

- available transmission capacity;
2. Identify the wind power plants that could potentially be connected to the HVDC line and quantify their wind energy output that could be transmitted via the HVDC transmission line;
  3. Assess the greenhouse gas emission reductions that could be achieved by enhancing the renewable integration via the DTLR approach;
  4. Evaluate and compare the financial benefits achieved by applying DTLR to the transmission network rather than conventional transmission capacity upgrading methods

## 1.3 Thesis Outline

**Chapter 2: Literature Review** This chapter includes a detailed review of the DTLR concept, its evolution, and past studies predominantly focused on its application in AC systems. A summary of HVDC transmission technology and its role in accommodating renewable energy sources, establishing the path for the identified research gap: the need to apply DTLR to HVDC transmission corridors.

**Chapter 3: Methodological Framework for DTLR Calculation and Wind Energy Assessment** This chapter provides a comprehensive technical foundation to explain the in-depth calculations performed in this research. Initially, the concept of ampacity is explained in this chapter along with the applicable standards. Later, the methodology employed to determine the real-time thermal capacity of transmission lines is explained. It involves the heat balance equation and wind energy calculation methodologies with the variables and parameters considered.

**Chapter 4: Dynamic Thermal Line Rating & Wind Power Generation** This chapter begins with presenting the study system utilized in the research study along with the meteorological data collection process and the calculation methodology

to implement DTLR in HVDC transmission corridors to reduce greenhouse gas (GHG) emissions. The chapter concludes with a close look at the results uncovered, followed by a discussion.

**Chapter 5: Economic Analysis** This chapter compares the financial benefits of the conventional line upgrading method with the method of applying DTLR. The annual revenues are calculated for each method and compared to understand the optimal solution for enhancing the capacity.

**Chapter 6: Conclusion & Future Work** The final chapter provides the conclusion of the entire thesis, summarizing key findings and emphasizing the contribution of the study. Further, the gaps in existing knowledge are identified and presented for future research in this specific area.

# Chapter 2

## Literature Review

### 2.1 Dynamic Thermal Line Rating (DTLR) Technology Overview

Research on overhead conductors which also leads to the topic DTLR goes back to the period before World War 2 [16]. Around this time, several studies were developed regarding heat transfer of conductors in still air but the major experiment including forced convection of conductors took place in 1930 by Schurig and Frick [17]. The results were used until recently however, the actual behavior of wind speed, direction, and gustiness made it challenging to accept their observed results. Wind tunnels were used as a common practice to study heat transfer from smooth and finned cylinders. In 1949, Hutchings and Parr took a step forward by using the same technique to study the heat transfer from stranded conductors under controlled conditions and then to determine the continuous ratings. Since then, there have been several groups studying the relationship of heat balance of overhead conductors. In 1959, House and Tuttle investigated the current temperature characteristics of ACSR conductors [18] where a current-carrying capacity formula was derived considering the conductor's heat loss and heat gain due to the effects of wind, solar radiation, ambient temperature, and surface conditions. Current carrying capacity(CCC) curves have also been constructed to observe the behavior of the CCC for various surface and ambient conditions and wind velocities [18]. This method of calculation considers all

the important factors without unnecessary simplifications. Hence, it is the practice that is inspired by the working group of IEEE 738 -2012 standard [19] which will be demonstrated in chapter 3.

The concept of DTLR offers many benefits when it comes to the domain of power transmission. This technology is an alternative method to increase the transmission capability of existing transmission systems [20]. The traditionally employed SR of the line is calculated based on worst-case weather conditions that sometimes are too conservative. Since the actual line ampacity depends on time-varying factors such as wind and solar radiation, taking into account real-time conditions will help to enhance the maximum allowable current of the line. There have been many studies conducted on applying DTLR in different power system scenarios. Some studies have found that employing DTLR in their systems enables the reduction of curtailment of wind power, lowers the electricity supply cost, and efficient operation of the system [21]. Further, this will help in transmission line congestion management by providing insights into real-time power line capacities and system bottlenecks to prevent the lines from getting thermally overloaded [22, 23]. This approach not only improves the system's overall efficiency but enables to integration of more renewable energy into the system utilizing the existing infrastructure [24].

## **2.2 Previous studies on DTLR**

With the daily increase in electricity demand, transmission system operators are facing the challenge of utilizing more capacity for the transmission lines. This has become a challenge to most of the countries in the world. Therefore, many countries have been studying and implementing new technologies to improve their transmission capacities.

There have been previous studies conducted before the 1970s regarding exploring the thermal capacity of the conductors. However, the article, "A new thermal rating approach: The real-time thermal rating system for strategic overhead conductor

transmission lines” [20], which was published in 1977 is known as the first academic article which is based on applying the thermal rating of the overhead conductors using real-time weather conditions. Since then, Table 2.1 summarizes some of the significant studies and pilot projects that have been carried out on the subject;

**Table 2.1:** Previous studies and pilot projects on DTLR

Year	Study
2008	The study explains an application of DTLR to a 132 kV double circuit transmission line in England, which connects Boston and Skegness. The dynamic rating was calculated based on meteorological data and it is found that 20% to 50% more wind energy can be incorporated. Four Power Donuts were installed to directly monitor the temperature of the line. The system is built so that it can coordinate the DTLR value with generation automatically. [25].
2011	A pilot experiment for a sag monitoring device known as ‘Ampacimon’ was conducted for a 400 kV twin conductor line in France. The system can interpret the line sag only by vibration analysis without needing any weather data or line data. Real-time line ampacity was calculated incorporating the measured sag measurements and most of the time it resulted in the line having extra capacity than the static rating at least by 20% [26]
2012	A study was conducted by German TSO based on two different DTLR methodologies; measuring the direct temperature of the conductor using SAW units and taking the weather station measurement. Results elaborate that determining DTLR from weather data is accurate up to a certain limit. They have also employed DTLR to a 380kV system to increase the rating to 3150 A. The study showed that once the DTLR is considered in the operation, a significant improvement in the rating can be observed which results in technical and economical benefits [12].
2013	A case study was conducted for one of the double-circuit transmission lines in Korea to analyze the benefits of using DTLR. They have investigated if a fault occurs in one of the circuits and how safely can the healthy circuit carry the total power. The results found that the maximum allowable load can be increased up to 135% [27].

2014	New York Power Authority, U.S.A, two DTLR demonstration projects were installed in Texas and New York in the year 2014. One has implemented the Nexans, CAT-1 systems to a heavily loaded transmission line in New York to optimize the power flow and assess the potential synergies between DTLR and phasor measurement unit (PMU). The other project is installing DTLR measuring units to five heavily loaded 138 kV lines in Texas [11].
2015	Idaho National Laboratory in collaboration with Alberta TSO, Altalink, have conducted a study on DLR. A weather-based DLR system called GLASS was used to calculate the dynamic rating which is based on IEEE 738. Precise wind data between weather stations were acquired by incorporating Computational Fluid Dynamics (CFD). The model ampacity calculations showed an error of about 6%. Multiple areas were selected to conduct the study finally concluding a minimum of 22% increase in ampacity 76% of the time [5].
2016	The report ‘Smart Grid to Enhance Power Transmission in Vietnam’ thoroughly describes how the DLR is applied in USA transmission networks and their gained benefits. Therefore, they have considered DLR technology as a tool to improve their smart grid operations and plans and how it can elevate the system operations with rapid increases in loads [28].
2017	A study was conducted on short-term forecasting of the line ampacity. The allowed maximum line current was calculated according to CIGRE standards for the next one to four hours. Special attention was given to predicting the wind speed/direction as it is more time and space-varying than the other parameters. Various models to predict wind data, including standard ARIMA, ARIMA as a state-space model, and simple state-space models with Kalman filtering, were tested and the most suitable methods were identified [29].
2018	The concept of DLR is applied for 35kV and 10kV overhead distribution lines in the Pudong power grid. Enhancing the power supply of the heavy-loaded lines and maximum utilization of the existing assets were the long-term goals of this study. An operational test was conducted for the line during the summer peak, it was found that the line can boost its capacity by about 20% more [30].

2020	A pilot project was conducted on DLR by the utility operator in Malaysia, for the critical 275kV Segar–Pantai–Ayer line. The DLR sensors were installed in two spans Span#1 (Tower 25–26) and Span#2 (Tower 48–49) while the paper discussed detailed studying the Span#1. Data analysis further showed that the system can increase the capacity 10% to 50% than the static rating 95% of the time and no major operational issues or maintenance were needed [31].
2022	The study delivers a comparison of two conductor thermal monitoring sensors highlighting their properties, measurements, and results. It further introduces a novel concept for DLR based on artificial neural networks and discusses its advantages over power line rating and thermal tracking. A significant finding of the concept was that it can independent capacity calculation from the sensor inputs over time. This concept provides not only technical significance but also economical [32].

The majority of existing research on this topic has focused predominantly on employing DTLR in AC systems and its presence in DC applications is limited. Borbáth et al. [14] discuss how the dynamic capacity of HVDC interconnectors can allow HVDC system operators to increase their profits and provide faster investment recovery. However, a thorough investigation of the theoretical understanding of how dynamic rating is achieved in HVDC interconnectors has yet to be conducted.

### 2.3 Applications of DTLR in Wind Power Integration

Electricity is one of the most important energy sources that play a major role in people’s lives since it is known to be efficient and reliable. Its portion of the world’s ultimate consumption of energy is predicted to increase from 20 % today to 22 % - 28 % by the year 2030 as depicted in the 2022 World Energy Outlook report [33]. Two-thirds of the world’s population resides in emerging markets and developing countries. As with the upcoming population settlements in those regions, countries should think about how they can meet their energy demands in the most eco-friendly and economical way [34]. In this context, as the electricity industry is a major

contributor to greenhouse gas emissions, utility companies are considering innovative solutions to minimize the impact on the environment.

As a solution to that, electric utilities have been planning on increasing their renewable energy generation into the generation mix. Fossil fuels, renewable energy, and nuclear power generated approximately 83.1%, 12.6%, and 4.3% of global energy consumption in 2020, respectively [35]. Hydropower, wind, solar, bioenergy, and geothermal come under the category of renewable energy sources. Among those, wind and solar have the highest potential for growth due to their lower construction period and large-scale expansion [35].

The move towards renewable energy production has given significant attention to wind power generation which is an eco-friendly solution to deriving energy from fossil fuels. In China, it is estimated that there has been a 35% growth in wind power generation [36]. According to a report by the Federal Ministry of Economic Affairs and Climate Action [37] the German government is planning to add 70 GW of wind energy to their system by 2045. A report published by North American Electric Reliability Corporation (NERC) [38], predicts roughly 260,000 MW of renewable energy will be added to the grid over the coming ten years, and 96% of that will be wind energy. Likewise, there are many examples available where most of the countries are shifting their focus towards harnessing wind energy.

The shift towards renewable will also raise doubt about the adequacy of the existing transmission infrastructure. Several measures can be taken to address the issue of insufficient transmission capacities including (1) strategically placing energy storage facilities to balance out the power in-feed and demand [39], (2) employing other energy carrier options such as hydrogen to alleviate the stress on the grid [40], (3) optimally utilize existing grid infrastructure to increase the capacity which is affordable and non-invasive.

Dynamic thermal line rating, as discussed in section 2.1, is such a technique that allows cold weather and wind to cool down the overheated transmission lines increas-

ing its thermal capacity [8]. Therefore, there is a correlation between wind energy and the thermal rating of the lines. When integrating wind power into the grid, the allowable capacity of the line can be enhanced when DTLR is taken into account rather than the SR [41]. This method has been widely discussed in many recent studies in various geographical regions as a means of improving their renewable generation contribution to the grid, e.g. Ireland, the United Kingdom, Canada, Spain, and Germany [5, 11–13].

A field study was conducted in N. Ireland to develop a statistical model to calculate dynamic line rating for a wind-intensive area [13]. This model can calculate the conductor temperature using line current and weather data. Two 110 kV single circuits from Omagh to Dungannon were selected to conduct the field study. Ten line monitoring locations were selected which are most prone to overheat during operation. Weather data was measured by the weather monitoring device, and conductor current and temperature were measured by an FMC sensor. Schell et al. [42] presented a situation in Belgium in which the Belgian TSO was in the need to add more wind power to their 70 kV network which is already saturated with the traditional calculations. Expanding the network at the moment was also not possible due to the budget issues. At first, they implemented an ANM (Active Network Management) which limits the output of the wind farms to ensure network safety. However, even if it provides the solution it reduces the involvement of renewable energy to their generation mix. Therefore they have implemented the DTLR to maximize the utilization of the existing network while minimizing the wind curtailment and increasing the network efficiency. A study employing dynamic line rating to utilize more wind power to the national grid in the Humber Estuary region, England presents a probabilistic modeling of wind output uncertainties based on historical data and suggests optimal locations for temperature monitoring [43]. Talpur et al. [44] investigate dynamic rating calculation for a 130 kV sub-transmission system owned by Fortum Distribution on how much further the conductor can be loaded up to its actual maximum capac-

ity. The study was extended to check the feasibility and best location to integrate a 60 MW wind power park to the same line. Teh and Cotton [45] introduce a new approach to evaluating the influence of a dynamic line rating system on the reliability of wind-powered networks. Findings suggest that DTLR systems are beneficial when there is a higher demand. Banerjee et al. [46] suggested an enhanced methodology for evaluating the power system's scheduling capacity considering variations in line ratings due to intermittent wind power. When applied to a test network, the suggested approach using DTLR helps integrate more wind power during network congestion.

In conclusion, combining renewable energy with dynamic line rating presents a promising future for enhancing the power systems' performance and reliability. The relationship between wind energy and dynamic rating holds the possibility of integrating more renewable energy while reducing network congestion.

## **2.4 HVDC systems overview**

### **2.4.1 History of HVDC**

In the early stages of electricity grids, the transmission distances were short and also the distribution voltages were low. Even the first commercial generators were operated by DC same as the distribution networks [47]. After recognizing the benefits of electrical energy, the electricity demand was raised and the electrical utilities were in the need to transmit electrical energy to longer distances. Therefore the the technology of DC transmission which was introduced by Thomas Alva Edison was not sufficient for the entire audience [48].

In 1883 Nikola Tesla was granted a patent for his 10 years of experiment on AC [47]. This was one of the turning points in the electrical industry which then was the base for many developments. However, the choice between AC and DC transmission since the 1880s led to the famously known "War of the Currents". On one side, Thomas Alva Edison supported entirely on the DC distribution network; on the other side,

George Westinghouse and Nikola Tesla were rooting for the AC distribution. However, by the 1890s due to limitations in DC technology such as transmission distances, difficulty in voltage transformation, higher losses, and costs, it was replaced by AC transmission [49].

However, while AC transmission has become popular, engineers did not stop seeking methods to explore technologies for DC transmission [47]. Out of many reasons to choose HVDC transmission, the following two reasons stand on top of that list. First, establishing a reliable AC transmission is not feasible when there is a connection between two terminals that operate at different frequencies or phase angles. In such scenarios, frequent tripping may be observed due to unacceptable power flow in the line. The second reason is that costs occurring due to additional terminal equipment in HVDC systems are justifiable for long-distance transmission through the savings achieved from the HVDC conductor systems [47]. Increase in energy demand and the requirement for more generation stations, limitations in AC transmission were identified. With the development of mercury arc valves, the first HVDC connection was commissioned in Gotland in 1953. Since then, many applications using mercury arc valves have come into operation. Nelson River Bipole 1 was the last application to use mercury-arc valves.

Following the mercury arc valves era, thyristor valves were introduced in 1957 making HVDC transmission a promising technology [50]. Later on, most of the mercury arc valve-based converters were replaced by thyristors, and new HVDC projects were constructed using thyristor-based converters. With the development of the HVDC converters by the time 1999, the thyristor valves were improved up to Insulated gate bipolar transistor (IGBT) switches.

### **2.4.2 HVDC Converter Technologies**

A basic illustration of an HVDC link is depicted in 2.1. At the sending end, the AC power is fed via the transformer and is then converted to DC power by the rectifier

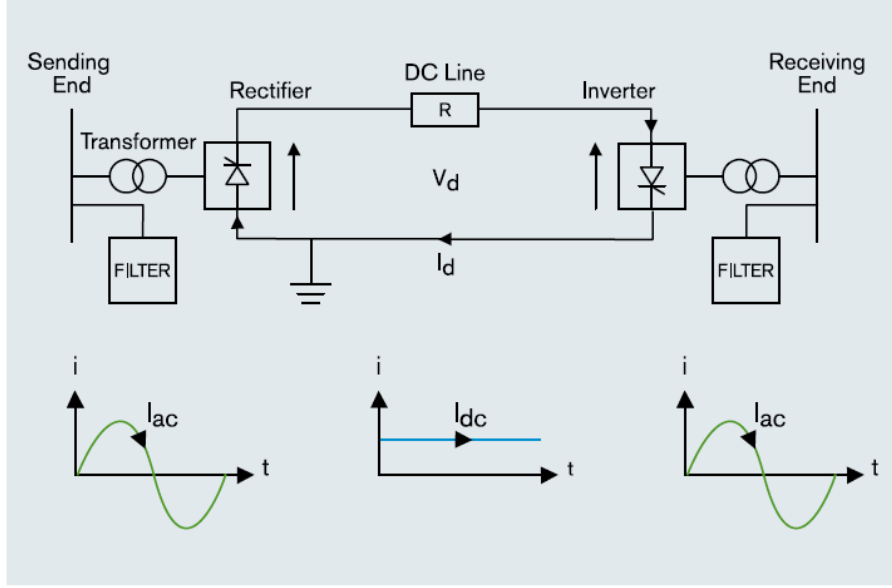


**Figure 2.1:** Simple representation of an HVDC link [51]

station irrespective of the frequency and phase of the AC supply. The converted DC power is then transmitted through the transmission link which is usually an overhead conductor, submarine cable, or a DC bus-bar. Then at the inverter station, the DC power is converted back to AC power and that power is transmitted through the receiving end AC network [51].

In HVDC transmission systems, converters are one of the key components in the systems that ensure AC-DC conversion and efficient power transmission. Two converter technologies are being used in HVDC transmission; line-commutated Current Source Converters (CSC) and self-commutated Voltage Source Converters (VSC) [52].

Line-commutated converters (LCC) are the most popular and well-established technology in the AC-DC conversion process in long-distance transmission [53]. This technology falls under CSCs that operate on AC system line parameters. The fundamental component involved with this technology is the Graetz Bridge which is a three-phase full-wave bridge comprised of six controlled thyristor valves [52]. The switching frequency of the thyristors are equal to the 50-60 Hz line frequency [54]. The requirement of harmonic filtering during commutation is reduced by employ-

ing 12 pulse converters in modern HVDC technology. However, the LCC process will always absorb reactive power since it operates with the AC current lagging the voltage.

VSC technology was first introduced in 1997 by ABB for the 3-MW project, Hällsjön- Grängesberg test link in Sweden [55]. Unlike LCC, VSC does not depend on the AC system to produce AC voltage. The fundamental structure of VSCs begins with two-level converters similar to the six-pulse bridge in LCC. Thyristor switches in LCC are replaced by IGBT devices in this technology with an inverse parallel diode connected to each IGBT [56]. This technology can control the active and reactive power independently of each other [52]. The following are different types of VSC technologies which has evolved with time [57]:

1. Two-Level VSC [First generation]
2. Three Level Diode Neutral Point Clamped (NPC) or Three Level Active NPC
3. Two Level with Optimum Pulse-Width Modulation (OPWM)
4. Cascaded-two Level Converter (CTL)
5. Modular Multi-Level Converter (MMC) [Latest generation]

### **2.4.3 HVDC Link Configurations**

Different types of configurations can be used when connecting two AC networks via an HVDC link. Following are the main four types:

1. Monopolar Link

There is only one conductor at a higher DC voltage in monopolar HVDC links. Another conductor is used as the ground return unless there are any environmental restrictions. In that case, the earth or sea can be the return path. This configuration is more suitable for long-distance transmission, especially for submarine cables. However, one drawback of this configuration is, that if there is

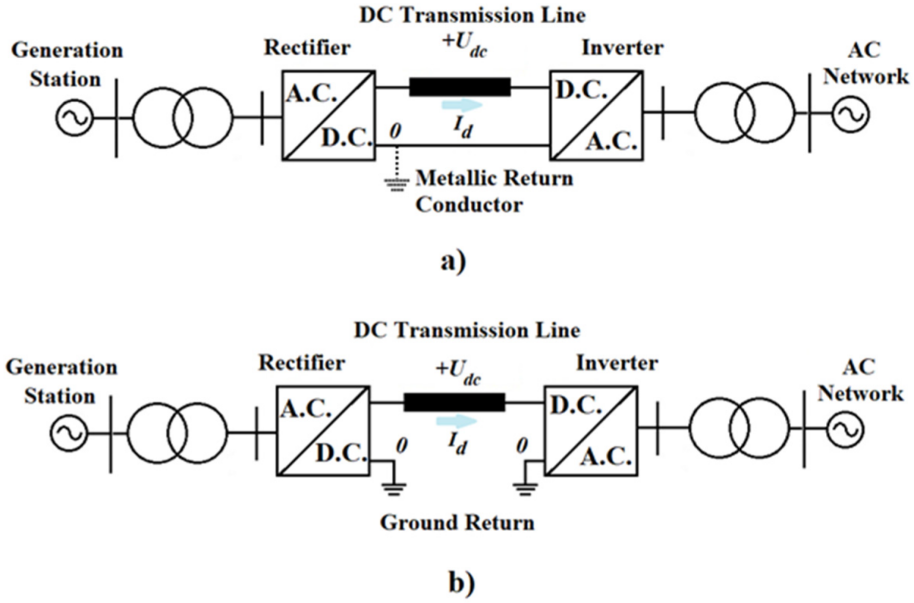


**Figure 2.2:** Monopolar link with a) Metallic return b) ground return [58]

any malfunction will result in the loss of the whole transmission capacity [14, 58, 59].

## 2. Bipolar Link

The bipolar configuration is a combination of two monopolar systems. Each side of the link consists of two equal-sized converters connected in series. The midpoint of the two sides is either connected via a metallic return or ground as the return path. During a converter's fault, the system can still operate with only half of the capacity lost by utilizing the metallic return as the return path [14, 58].

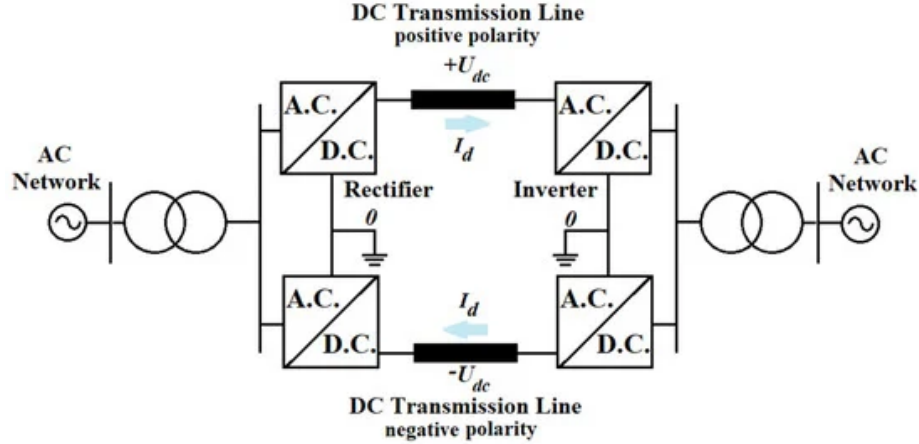


**Figure 2.3:** Bipolar link with ground return [58]

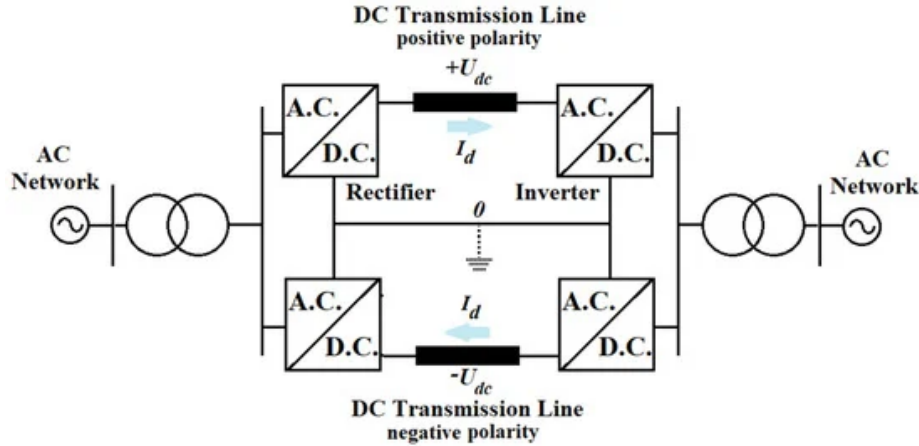


**Figure 2.4:** Bipolar link with metallic return [58]

### 3. Back-to-Back Link

Back-to-back configuration can be introduced as the simplest among the configurations. Both inverter and rectifier stations are located in the same building or close to each other. Hence the DC link is a short distance. This type of configuration is used when two AC systems are to be connected which are not synchronized or run at different frequencies [14, 58, 59].

### 4. Homopolar Link

Homopolar links are also the same as bipolar links, but the difference is that both poles in this configuration have the same polarity. Usually, both poles will

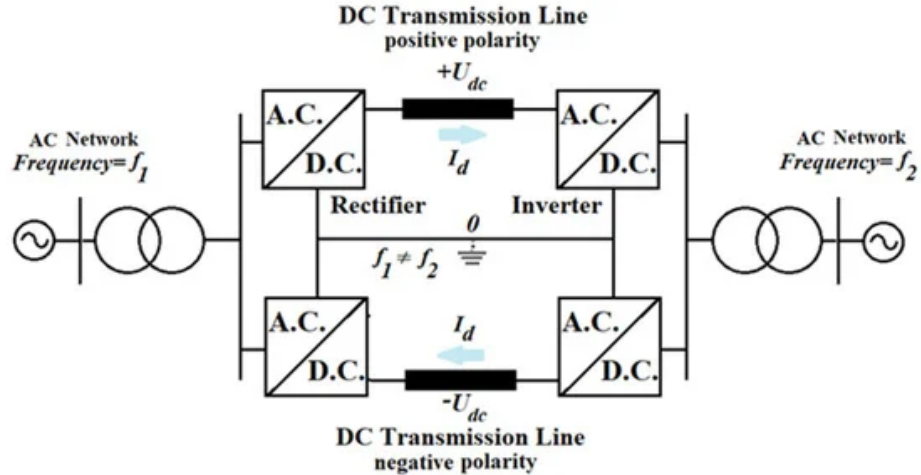


Figure 2.5: Back-to-Back configuration[58]

be in negative polarity [60].

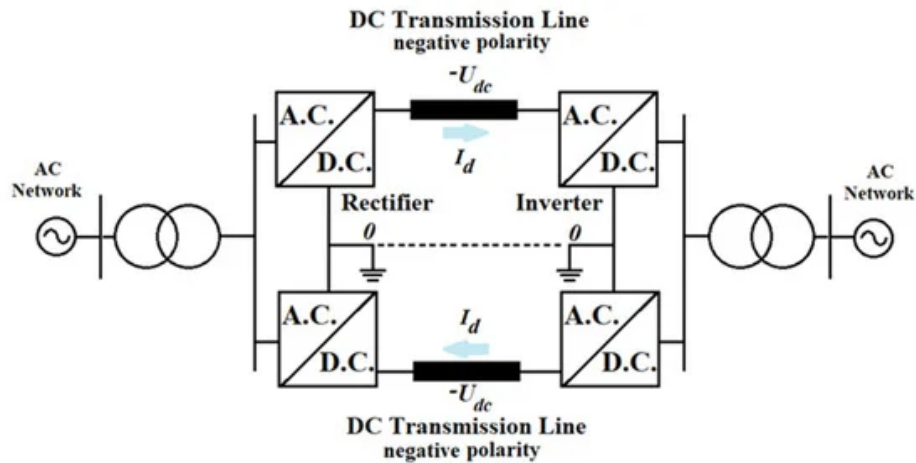


Figure 2.6: Homopolar Configuration[58]

## 2.5 Role of HVDC in Renewable Energy Integration

Throughout the past century, HVAC was the predominant transmission system used to transmit electrical power from generation stations to distribution centers often spanning hundreds of kilometers. The main advantage of this technology consists of relatively low-cost and simple equipment such as transformers, and circuit breakers as compared to the expensive and complex converter systems in HVDC [61]. However,

when it comes to transmitting bulk power over long distances, HVAC comes with significant disadvantages including the increase in losses. As the line length increases, the line reactance increases resulting in increased reactive losses. Further, the losses due to the skin effect of the line, corona effect, and radiation losses are also present in HVAC systems [62]. Therefore, HVDC long-distance bulk power transmission is emerging as an alternative solution for HVAC.

The world's shift towards higher penetration of renewable energy necessitates significantly improving the grid infrastructure including transmission and distribution networks [63]. Additionally, the substantial growth in renewable energy also includes offshore sources specifically large-scale wind power plants which are located considerably at a long distance from the demand centers. This widespread nature of renewable energy resources increases the demand for long-distance interconnection between different geographical locations and bulk power transmission [64]. Transmission lines based on HVDC technology allow to transmission of the generated power from offshore plants such as wind, solar, and tidal which are offshore or in distant locations to onshore demand centers with minimum losses [65, 66].

Wind energy is given priority status in a majority of the world through feed-in tariffs, which provide grid access and competitive guaranteed feed-in pricing [67]. The total cost of a wind energy connection is typically divided into two categories; route cost and terminal cost for comparison and analytical purposes [68, 69]. HVAC holds the advantage over HVDC regarding terminal costs due to the existence of expensive converters in HVDC terminals. Also, HVAC has the benefit of short-distance transmission due to its lower terminal costs until a certain limit. However, beyond that limit the route costs favor HVDC. For wind farms within 50–75 km, HVAC is the most straightforward and cost-effective connection method. However, if the distance exceeds 100–150 km, HVDC transmission may be the only viable option [70].

Various significant topics related to wind energy integration through HVDC trans-

**Table 2.2:** LCC-HVDC projects for renewable energy integration in China [77]

Project	Capacity (MW)	Rated voltage (kV)	Transmission line length (km)
Hami–Zhengzhou	8 000	$\pm 800$	2 210
Jiuquan–Hunan	8 000	$\pm 800$	2 383
Xilin Gol League–Taizhou	10 000	$\pm 800$	1 628
Jarud Banner–Qingzhou	10 000	$\pm 800$	1 234
Shanghaimiao–Shandong	10 000	$\pm 800$	1 238
Zhundong–Wannan	12 000	$\pm 1\ 100$	3 324
Qinghai–Henan	8 000	$\pm 800$	1 587
Shaanxi–Wuhan	8 000	$\pm 800$	1 137

mission are covered in an extensive amount of literature, including technical and economic analysis, the feasibility of different topologies, grid connection methods, loss evaluations, operation and control strategies, etc [70–76]. In this context, not only off-shore but HVDC has also been utilized in onshore renewable energy integration. China has multiple examples of wind energy integrated via HVDC systems. China with its demand centers located in central and eastern regions primarily its onshore wind and solar resources concentrated in the north, northern, and northeast regions [77]. Due to the diverse distribution of generation sources and load centers, long distance transmission is imperative. As a result, LCC-based HVDC is widely used in China for the extensive use of onshore renewable energy. Table 2.2 shows a few of China’s LCC-HVDC projects that are under construction or in operation.

## 2.6 Key outcomes of the literature review

In conclusion, the increase in electricity demand resulted in the improvement of existing transmission and distribution infrastructure as well as the need for long-distance transmission. When it comes to long distance transmission, the the HVDC systems surpassed the benefits of HVAC systems. Therefore, ways to improve the HVDC

transmission infrastructure are crucial at this point. The overview of DTLR coupled with the examples of past studies, establishes a better understanding of the evolution of the technique and how it has been used in real time networks. The findings show that incorporating DTLR can lead to a reduction in wind power curtailment, a decrease in electricity supply costs, benefit transmission line congestion management, and an overall enhancement in system efficiency. However, a notable gap in the literature surfaces—the existing studies on DTLR predominantly experiment with AC systems. This study steps into the spotlight by bringing in a new approach—adding DTLR to HVDC transmission corridors intending to maximize the utilization of their capacity and facilitate increased integration of renewable energy.

# Chapter 3

## Methodological Framework for DTLR Calculation and Wind Energy Assessment

### 3.1 Conductor Rating and Ampacity

The concept of ampacity emerged through research focused on expanding the capacity of the transmission lines. It refers to the maximum electrical current a conductor can handle continuously without experiencing deterioration. Several elements, including the conductor's construction and design, the condition of the surrounding environment, and the line's operating circumstances, limit the ampacity of a line [78].

Ampacity is divided into two categories: static and dynamic [13, 79, 80]. Static ampacity also known as SR is calculated considering the worst-case conditions for both the conductor and its environment which is too conservative. This can result in low efficiency of the grids.

In contrast, the dynamic rating considers the fluctuation of the grid and its environment including ambient temperature, wind, solar radiation, etc. By measuring the conductor's behavior such as heating and cooling effects in real-time, the maximum instantaneous real current that the conductor can carry without violating the safety limits can be determined [81, 82]. That allows the grid to operate more efficiently than when using the static rating.

Deterministic techniques or probabilistic methods have been used to measure or estimate the operational parameters to determine the ampacity. The techniques used for determining the ampacity and temperature of the conductor are outlined in standards published by the Institute of Electrical and Electronics Engineers (IEEE) [19] and the International Council on Large Electric Systems (also known as the Conseil International des Grands Reseaux Electriques, CIGRE) [15].

## 3.2 Overview of relevant technical standards

The current versions of the two standards provided by the two institutions are the IEEE for Calculating the Current-Temperature Relationship of Bare Overhead Conductors (IEEE Std. 738-2012) [19] and Guide for Thermal Rating Calculations of Overhead Lines (CIGRE WG B2.43) [15]. Both methods determine the thermal rating of the line based on the heat balance between the conductor and the environment [83]. It assumes that the heat gain is equal to the heat loss from the conductor. Also, both of them consider the environmental parameters such as wind velocity, wind direction, solar radiation, ambient temperature, etc [84]. However, they both have a different way of calculating the heat balance equation. The versions of the heat balance equations used by CIGRE WG B2.43 [15] and IEEE Std. 738 -2012 [19] are presented in eq. 3.1 and eq. 3.2 respectively.

$$P_c + P_r + P_w = P_s + P_j + P_m + P_i \quad (3.1)$$

$$P_c + P_r = P_s + P_j \quad (3.2)$$

Where:

$P_c$  convective cooling

$P_w$  evaporative cooling

$P_r$  radiative cooling

$P_j$	joule heating
$P_s$	solar heating
$P_m$	magnetic heating
$P_i$	corona heating

Observing eq. 3.1 and eq. 3.2, it is evident that the CIGRE method comprises three additional components evaporative cooling ( $P_w$ ), magnetic heating ( $P_m$ ), and corona heating ( $P_i$ ) in contrast to IEEE Std. 738 method. The IEEE Std. 738 method excludes these parameters as they typically have a negligible effect on ampacity ratings. Nevertheless, the IEEE Std. 738 takes magnetic heating into account by incorporating the AC resistance of the conductor at both low and high temperatures [85].

However, it is found that corona heating becomes accountable only when the convective and evaporative cooling are high. Also, heat transfer through evaporation and corona happens randomly and, as a result, should be addressed using a probabilistic approach [86]. Therefore, both standards generally agree to disregard both evaporation and corona heating due to their probabilistic nature.

The main differences between the two standards are [87]:

1. Calculating solar heating in IEEE Std. 738 involves taking the sun's position by considering the hour and date of the year while CIGRE WG B2.43 adopts a sophisticated algorithm employing direct, diffuse, and reflected radiation.
2. IEEE Std. 738 adopts the convective cooling algorithm by McAdams correlations which relies on the Reynolds number while the CIGRE WG B2.43 employs the Nusselt number in Morgan correlations.

There exist studies that have outlined the differences between IEEE Std. 738 and CIGRE WG B2.43 standards and how their differences impact the thermal rating results. The experimental validation in the work of Abbott et al. [88] demonstrates both standards can predict the conductor temperature with significant accuracy with

a mean absolute error of  $0.70^{\circ}\text{C}$ . The study by Arroyo et al. [84] calculates the temperature of an LA 280 Hawk type, used in a 132-kV overhead line estimated by the two standards. The results show that both standards give comparable results with minor differences due to the variations in calculating the solar heat gain and convective loss. As indicated by certain studies, both the standards are used in the same range and the accuracy is sufficient enough with variations in the values typically between 5-15% but no more than that [85].

CIGRE WG B2.43 standard consists of more complex and thorough analysis, sometimes it is not always essential to invest time in detailed calculations while the simple methods can yield sufficient results. Therefore, the choice between the two standards ultimately depends on the user's preference, data availability, and the purpose of the study.

### 3.3 Heat Balance Equation

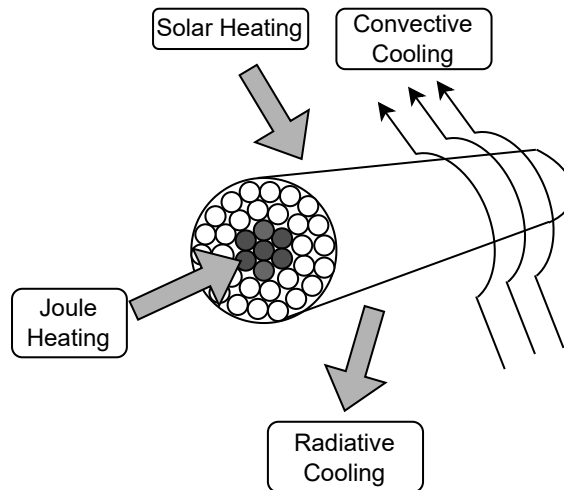


**Figure 3.1:** Heat balance of an overhead conductor

This section describes the thermal model of the bare overhead conductors and their parameters closely following the IEEE Std 738-2012 [19]. The equations are formulated to determine the dynamic line rating using real-time weather data and line loading. The core of the standard mentioned above is the heat balance equation which

comprises equalizing the conductor’s heat gains to its losses. When the conductor is in the “steady state” condition, the heat supplied to the conductor by Joule losses and solar radiation is equal to the heat dissipated primarily by convection and radiation to the surrounding atmosphere (see Fig. 3.1). Therefore the simplified steady-state heat balance equation can be written as;

$$\begin{aligned} \text{Heat Loss}_{\text{conductor}} &= \text{Heat Gain}_{\text{conductor}} \\ q_c + q_r &= q_s + q_j \end{aligned} \tag{3.3}$$

Where  $q_c$  and  $q_r$  are the heat losses from the conductor due to convection and radiation respectively while  $q_s$  is the solar heat gain and  $q_j$  represents heat gain by the conductor due to the joule heating of the conductor.

### 3.3.1 Convective heat loss ( $q_c$ )

Convective heat loss highly depends on the wind around the conductor and is one of the most important conductor cooling methods. When the convective cooling is low, the conductor temperature goes high. The value of the convective heat loss depends on a dimensionless parameter known as Reynold’s number as given in the equation :

$$N_{re} = \frac{D_o \times \rho_f \times V_W}{\mu_f} \tag{3.4}$$

This will depend on wind velocity ( $V_W$ ), dynamic viscosity of air ( $\mu_f$ ), and coefficient of thermal conductivity of air ( $K_f$ ). According to the IEEE Std. 738 [19], convective heat loss can be divided into two categories, one for still air conditions and one for wind speeds above zero. The magnitude of the highest value is taken to substitute in eq.(3.3).

#### 3.3.1.1 Natural convection

Natural convection happens when the wind velocity is zero also known as still air condition. The value of this depends on air temperature ( $T_s$ ), conductor temperature ( $T_a$ ), air density ( $\rho_f$ ) and conductor diameter ( $D_o$ ).

$$q_{cn} = 3.645 \times \rho_f^{0.5} \times D_o^{0.75} \times (T_s - T_a)^{1.25} \quad (3.5)$$

### 3.3.1.2 Forced convection

Heat loss due to forced convection mainly depends on the wind speed and direction. This is again classified into two categories; wind speeds lower than 4.47 m/s and speeds higher than or equal to 4.47 m/s. The loss at low wind speeds is calculated with eq.(3.6).

$$q_{c1} = K_{\text{angle}} \times [1.01 + 1.35 \times N_{re}^{0.52}] \times K_f \times (T_s - T_a) \quad (3.6)$$

Similarly, the loss at high wind speeds is calculated with the help of eq.(3.7).

$$q_{c2} = K_{\text{angle}} \times 0.754 \times N_{re}^{0.6} \times K_f \times (T_s - T_a) \quad (3.7)$$

During lower wind speeds the maximum among the natural and forced convection losses are used. In cases with zero wind speeds, there will be no heat loss due to forced convection, but the natural convection will act up and help cool down the conductor.

Also, to calculate the forced convection rate, the wind direction factor ( $K_{\text{angle}}$ ) must be calculated as in eq. (3.8). Where  $\phi$  represents the angle of the wind to the conductor axis.

$$K_{\text{angle}} = 1.194 - \cos(\phi) + 0.194 \cos(2\phi) + 0.368 \sin(2\phi) \quad (3.8)$$

The coefficient of thermal conductivity of air ( $k_f$ ), air density ( $\rho_f$ ), and air viscosity ( $\mu_f$ ) should also be calculated according to section 4.5 in IEEE Std. 738. They are all calculated at the air film temperature, which is the average between ambient temperature ( $T_a$ ) and maximum allowable conductor temperature ( $T_s$ ):

$$T_{\text{film}} = \frac{T_s + T_a}{2} \quad (3.9)$$

$$K_f = 2.424 \times 10^{-2} + 7.477 \times 10^{-5}(T_{\text{film}}) - 4.407 \times 10^{-9}(T_{\text{film}})^2 \quad (3.10)$$

$$\mu_f = \frac{1.458 \times 10^{-6}(T_{\text{film}} + 273)^{1.5}}{T_{\text{film}} + 383.4} \quad (3.11)$$

$$\rho_f = \frac{1.293 - 1.525 \times 10^{-4} \times h_e + 6.379 \times 10^{-9} \times h_e^2}{1 + 0.00367 \times T_{\text{film}}} \quad (3.12)$$

### 3.3.2 Radiated heat loss ( $q_r$ )

Radiation heat loss happens when the conductor temperature rises above the temperature of the surroundings. The energy is transmitted from the conductor to the surroundings by radiation depending on the temperature difference. However,  $q_r$  has the least impact on line ratings.

$$q_r = 17.8 \times D_0 \times \epsilon \times \left[ \left( \frac{T_s + 273}{100} \right)^4 - \left( \frac{T_a + 273}{100} \right)^4 \right] \quad (3.13)$$

### 3.3.3 Solar heat gain ( $q_s$ )

Similarly, the conductor's heat gain from solar radiation is calculated using eq. 3.14. It can be seen that the amount of solar energy received by the conductor mainly depends on conductor area ( $A'$ ), overall heat intensity radiated from solar and sky adjusted for elevation ( $Q_{se}$ ), solar absorptivity ( $\alpha$ ), and the conductor latitude ( $\theta$ ).

$$q_s = \alpha \times Q_{se} \times \sin(\theta) \times A' \quad (3.14)$$

where:

$$\theta = \arccos[\cos(H_c) \times \cos(Z_c - Z_1)] \quad (3.15)$$

### 3.3.4 Joule heat gain ( $q_j$ )

Joule heating also known as ohmic loss which is caused by the flow of current through the conductor converting the electrical energy into heat due to its inherent resistance is calculated based on the equations 3.16 and 3.17:

$$q_j = I^2 R_{T_{avg}} \quad (3.16)$$

where  $R(T_{avg})$  is the resistance of the conductor at the maximum operating temperature.  $I$  represents the conductor current that can bring the conductor to its maximum safe operating temperature under the given weather conditions.

According to the standard [19] the electrical resistance is calculated in a linear manner for the surface temperature of the conductor. For instance, if the conductor resistance values at high ( $T_{high}$ ) and low ( $T_{low}$ ) temperatures are available from the manufacturer's information, the resistance can be found at any other temperature ( $T_{avg}$ ) through linear interpolation using the specific equation 3.17.

$$R_{T_{avg}} = \left[ \frac{R_{T_{high}} - R_{T_{low}}}{T_{high} - T_{low}} \right] \times (T_{avg} - T_{low}) + R_{T_{low}} \quad (3.17)$$

Once all the parameters fulfill the heat balance equation in 3.3 is quantified, assuming a reasonable distribution of temperature across the conductor, the ampacity of the conductor can be expressed as:

$$I = \sqrt{\frac{q_c + q_r - q_s}{R_{T_{avg}}}} \quad (3.18)$$

When calculating the line rating for a long transmission line, the process starts by identifying the maximum allowable temperature of the conductor. Subsequently, the line is divided into sections as in Fig. 3.2, either by equal distance or at locations where weather parameters are available. Following this division, the rating for each section is calculated. Finally, the ampacity for the entire line is calculated with the minimum value taken from all the sections for the particular period under consideration:

$$A(t) = \min_i A_i(t) \quad (3.19)$$

where  $A_i$  is the conductor current rating at a given point  $i$ , during time  $t$  [89]. Thereby, the amount of actual power that can be transmitted by a DC transmission line can be quantified.

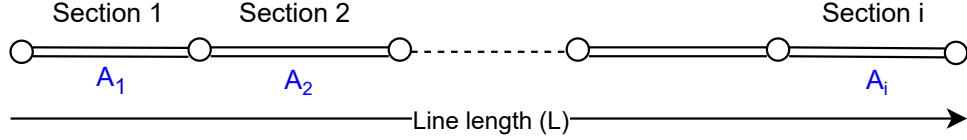


**Figure 3.2:** Transmission line divided into sections

### 3.4 Wind Energy

Kinetic energy stored in wind is a source for renewable energy generation which has a substantial global potential. It is estimated that there is around  $3 \times 10^{15}$  kWh of kinetic energy in the airflow of the atmosphere every year. Theoretically, the maximum usable energy from that is estimated to be around  $30 \times 10^{12}$  kWh/year, equivalent to approximately 35% of the global energy use [90].

In order to harness the kinetic energy from the wind, wind turbines are used and approximately 36% of the energy that sweeps the turbine can be transformed into electrical energy [91]. The useful power that can be extracted from the turbine can be assessed by calculation or by the turbine's power curve. To calculate the power output the equation expressed below can be used:

$$p(v) = \frac{1}{2} \rho A v^3 C_p \quad (3.20)$$

Where  $p(v)$  is the output power in W,  $\rho$  is the air density ( $1.28 \text{ kg/m}^3$ ),  $A$  is the swept area of the wind turbine blade ( $m^2$ ),  $v$  is the wind speed ( $ms^{-1}$ ),  $C_p$  is the coefficient of performance.  $C_p$  depends on the technology of the turbine and its

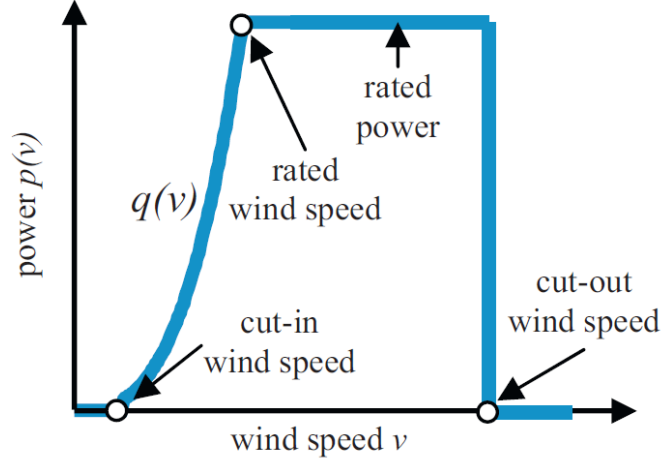


**Figure 3.3:** General representation of a wind turbine power curve [91]

controls [92]. However, according to the Betz law, this coefficient is limited and it says that the maximum a turbine can harness is  $16/27 \approx 59\%$  of the kinetic energy. It can be even lower in real world scenarios [93] and it can be calculated for large wind turbines as in eq. 3.21 [92]:

$$C_p(\lambda, \beta) = 0.73 \left( \frac{151}{\lambda_i} - 0.58\beta - 13.2 \right) \exp \left( \frac{-18.4}{\lambda_i} \right), \quad (3.21)$$

where  $\beta$  represents pitch angle and  $\lambda_i$  represents the tip speed ratio

$$\frac{1}{\lambda_i} = \frac{1}{\lambda + 0.02\beta} - \frac{0.003}{\beta^3 + 1}. \quad (3.22)$$

The power control of the turbine relies on adjusting  $C_p$  since  $A$  and  $\rho$  are constants of the turbine and wind speed  $v$  cannot be controlled.

Usually, the wind turbine's power output is illustrated in its power curve which establishes the relationship between the wind speed and corresponding power output [94]. Figure 3.3 shows a general representation of a wind turbine power curve. It is drawn by the manufacturer of the turbine according to the standards applicable to the specific country [91].

$$p(v) = \begin{cases} 0 & v < v_{ci} \text{ or } v > v_{c0} \\ q(v) & v_{ci} \leq v \leq v_r \\ P_r & v_r \leq v \leq v_{c0} \end{cases} \quad (3.23)$$

The relationship between wind speed and turbine output in the power curve can be articulated as in 3.23 [94] where,  $p(v)$ : electric power output (W),  $q(v)$ : non-linear relationship between power and wind speed,  $v_r$ : rated wind speed ( $ms^{-1}$ ),  $v_{ci}$ : cut-in wind speed ( $ms^{-1}$ ),  $v_{c0}$ : cut-out wind speed ( $ms^{-1}$ ),

The typical height of a meteorological station where the wind speed is measured is about 10m. However, the wind turbines have larger hub heights than 10m and the height differs from turbine to turbine. Therefore the values acquired from the meteorological station should be extrapolated to the turbine hub height when calculating the wind turbine output [95]. There are numerous extrapolation laws in the literature [96], and the power law equation expressed below is generally used in engineering studies [97].

$$\frac{v_2}{v_1} = \left( \frac{h_2}{h_1} \right)^\alpha \quad (3.24)$$

where,  $v_2$  is the wind speed to be calculated at the height  $h_2$ ,  $v_1$  is the wind speed measured at anemometer height  $h_1$  and  $\alpha$  is the Hellmann (or friction) exponent. Various authors have proposed several methods to calculate the exponent [96] nevertheless have used the expression created by C. G. Justus et al. [98] and it is given by:

$$\alpha = \frac{0.37 - 0.0881 \ln(v_1)}{1 - 0.0881 \ln\left(\frac{h_1}{10}\right)} \quad (3.25)$$

### 3.5 GHG Emissions From Electric Sector

The growth of electricity demand results in an increase in the amount of power generated from fossil fuels, which contributes to the increase in GHG emissions and climate change. As a consequence, electric power generation utilities pay significant attention to reducing emissions from existing power plants and increasing renewable energy generation [99]. Table 3.1 provides a comprehensive overview of GHG emissions over the life cycle of each type of generation technology. According to the table, coal-fired power plants are the second greatest contributor to  $CO_2$  emissions. In contrast, wind power stands as one of the most eco-friendly generation technologies, emitting only 3-22 g of  $CO_2$  per kWh.

**Table 3.1:** Average GHG emission over life cycle by each generation technology. [89]

Technology	Avg. $CO_2$ per kWh
Wood	1500 g
Coal	800-1050 g
Natural gas	430 g
Photovoltaic solar	60-150g
Nuclear	6g
Hydro	4 g
Wind	3-22 g

Table 3.2 lists the key pollutants generated by coal-fired plants which are not only  $CO_2$  but also other toxic materials such as mercury [89]. This emphasizes the urgency of switching to green energy sources and also the importance of research in addressing the challenges caused by conventional electricity production methodologies.

In the context of this research, these values are used to assess emission reduction by applying DTLR strategies to incorporate more renewable energy. This evaluation confirms the environmental impact of adding more renewables such as wind energy

**Table 3.2:** Key pollutants discharged by coal power plants. [89]

Compound	Avg. emissions per kWh
Carbon Dioxide ( $CO_2$ )	371.95 g
Sulphur Dioxide ( $SO_x$ )	2.72 g
Nitrogen Oxides ( $NO_x$ )	1.81g
Methane ( $CH_4$ )	476.27g
Mercury ( $H_g$ )	$4.08 \times 10^{-7}$ g

to the mix. The use of DTLR is an important enabling factor to minimize GHG emissions.

# Chapter 4

## Dynamic Thermal Line Rating & Wind Power Generation

### 4.1 HVDC system case study for DTLR analysis

HVDC technology has enormous potential in Canada, which is not surprising given its crucial position in the country's energy sector. Approximately 12 GW of current capacity is established in Canada utilizing the HVDC technology predominantly via the LCC HVDC converter technology [100]. Significant growth in the initiation of the HVDC market in Canada was witnessed in the 1980s and 2010s specifically with the introduction of the first VSC HVDC system which is known as the Maritime Link by ABB in 2018 [100]. Since then it has been proven from projects such as Manitoba's Nelson River Bipolar transmission lines, and Alberta's Eastern and Western transmission lines that Canada has a promising future ahead of it, filled with possibilities for growth and innovative supply of clean and renewable energy.

Identifying the potential of HVDC in Canada, the performance of the proposed approach is evaluated by conducting a case study for an HVDC transmission line in Alberta, Canada. The Eastern Alberta Transmission Line (EATL) and Western Alberta Transmission Line (WATL), are the two transmission corridors between the north and south of Alberta. Since southern Alberta is identified as more favorable for wind and solar, there is a need to transfer power for long distances from south to north. As recently HVDC is gaining more popularity in long-distance transmission

and renewable energy integration, this specific benchmark system is chosen to assess the effectiveness of implementing DTLR in HVDC transmission corridors.

#### 4.1.1 Study system

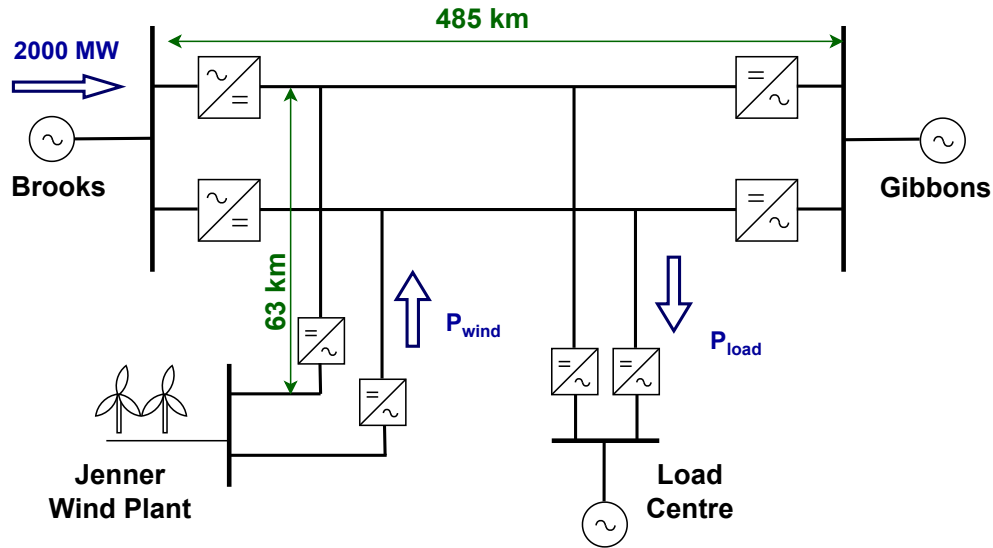


**Figure 4.1:** Study system configuration

The potential study system configuration is illustrated in Fig. 4.1. The system represents the EATL which spans 485 km and operates as a  $\pm 500$  kV HVDC link. The line is constructed between the Gibbons area, northeast of Edmonton, and the Brooks area Southeast of Calgary, as shown in Fig. 4.2. Currently, the line is operated as a 1000 MW monopolar system but conductors for a second pole have already been strung onto the transmission line so that it can be converted to a bipolar operation. This upgrade will effectively double the transfer capability when needed in the future [101]. Conductors that carry the power from EATL are 1590 ACSR Falcon wire with specifications provided in Table 4.1.

Renewable integration is carried out by incorporating the Jenner wind farm [102] as shown in Fig. 4.1. Jenner Wind Power Project (JWPP) is one of the many renewable energy projects planned to be added to Alberta’s electric system. It is located near the town of Jenner in southeast Alberta. The total project consists of 3 phases



**Figure 4.2:** Location map of EATL and Jenner wind farms

[102]: JWPP, JWPP2 and JWPP3. Among these, JWPP and JWPP3 are already in operation. JWPP2 will consist of 13 Enercon E160 turbines, each with a nameplate capacity of 5.49 MW, for a total capacity of 71.4 MW.

In the context of this study, several assumptions were deliberately used to simplify the case. It is taken into account that EATL is a  $\pm 500$  kV HVDC bipolar link that can transfer a maximum of 2000 MW power (1000 MW per pole). The power produced from JWPP2 is fed into EATL, even though they might be connected to the AC transmission in the actual scenario. The wind farm specifications considered for this study are provided in Table 4.2, while the turbine power curve is shown in Fig. 4.3 [103]. Further assumptions include that the power generated from the wind farm is delivered to EATL and harnessed at an intermediate point of the line. Additionally, it is assumed that the tap to the load center functions solely as an inverter in this study.

**Table 4.1:** Assumed HVDC line conductor parameters

<b>Parameter</b>	<b>Value</b>
Conductor type	1590 Falcon
Nominal Rating	1359 A
Inside diameter	13.08 mm
Outside diameter	39.22 mm
DC Resistance at 20°C	0.035433 $\Omega$ /km
DC Resistance at 50°C	0.0401 $\Omega$ /km
Absorptivity	0.8
Emissivity	0.8

**Table 4.2:** Jenner wind farm specifications

<b>Parameter</b>	<b>Value</b>
Turbine model	Enercon E-147
Number of turbines	13
Turbine rated power	5,000 W
Cut-in speed	2.5 m/s
Cut-out speed	25 m/s
Hub height	126 m

### 4.1.2 Meteorological data collection

In this study, the acquisition of accurate historical weather data is important to calculate the DTLR. Initially, consideration was given to all weather stations close to the EATL, identifying a total of 23 weather stations along and close to the line. In addition, the selection was narrowed down by choosing stations that provided all the necessary weather parameters essential for the investigation.

Consequently, six weather stations were chosen — Andrew AGDM, Brooks, Fleet AGCM, Killam AGDM, Pollockville AGDM and Vegreville — where comprehensive

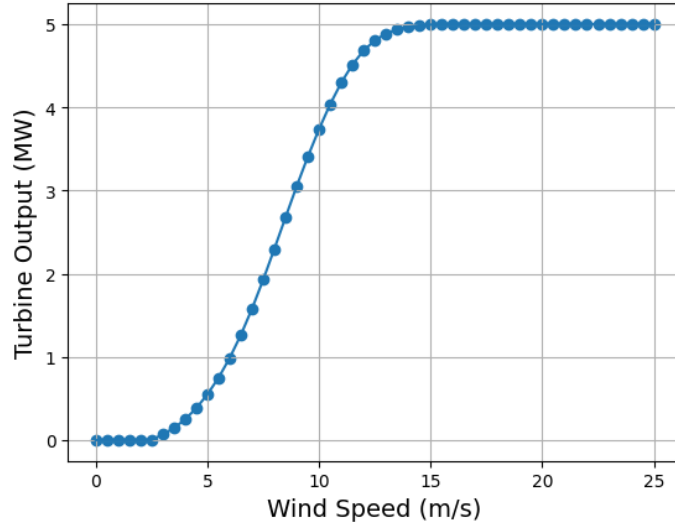


**Figure 4.3:** Power curve for Enercon E-147 5MW turbine [103]

meteorological data on ambient temperature in °C, wind speed (km/h), wind direction (°), and Solar Radiation ( $W/m^2$ ) were available. These data were acquired from the online web resource Current and Historical Alberta Weather Station Data Viewer provided by the Agriculture and Irrigation, Alberta Climate Information Service (ACIS) [104].

For the assessment of the wind energy production of the plant, the same ACIS platform was utilized [104]. Hourly wind data from the Atlee AGCM weather station, situated close to the JWPP2 wind farm location, were obtained to ensure accurate calculations.

### 4.1.3 Overall methodology followed for DTLR calculations and wind energy assessment

Fig. 4.4 presents the overall methodology adopted for calculating the DTLR, GHG emission reductions, and wind energy generation. By adopting the weather station selection approach in section 4.1.2, the HVDC transmission line was divided into five distinct sections, as prescribed in Fig. 3.2. Hourly weather data for both summer and winter seasons were procured for each designated weather station. The summer period spans from May 1<sup>st</sup> to October 31<sup>st</sup> while the winter period covers from November 1<sup>st</sup>

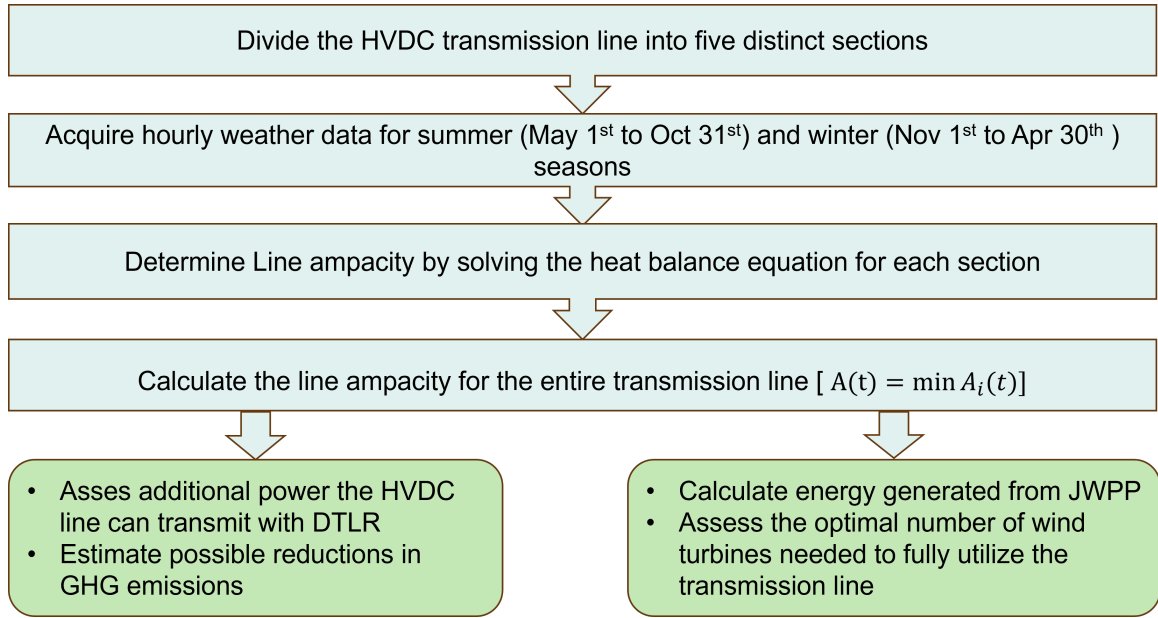


**Figure 4.4:** Overall methodology

to April 30<sup>th</sup> each year. Subsequently, the line ampacity was determined by solving the heat balance equation (3.3) for the maximum conductor temperature of 70°C.

In this study, we performed two key calculations to assess the impact of DTLR on the EATL. Initially, the DTLR technique was applied by incorporating the acquired weather data and heat balance equation (3.3). This allowed determination of the total power the HVDC line can transmit with DTLR, along with the additional power achievable beyond the nominal line rating. The subsequent estimation considered that additional power is solely produced by renewable energy sources connected to the line, estimating possible reductions in GHG emissions through the replacement of coal-fired power facilities with renewable energy.

The second calculation explored the integration of the JWPP2 plant with the HVDC line, as depicted in Fig. 4.1. The amount of energy that could be generated by the plant was calculated considering the wind data available from the nearest weather station to the plant (Atlee AGCM). Leveraging the previously calculated DTLR, the optimal number of wind turbines needed to fully utilize the transmission line without the need for additional infrastructure development was then determined.

## 4.2 Results

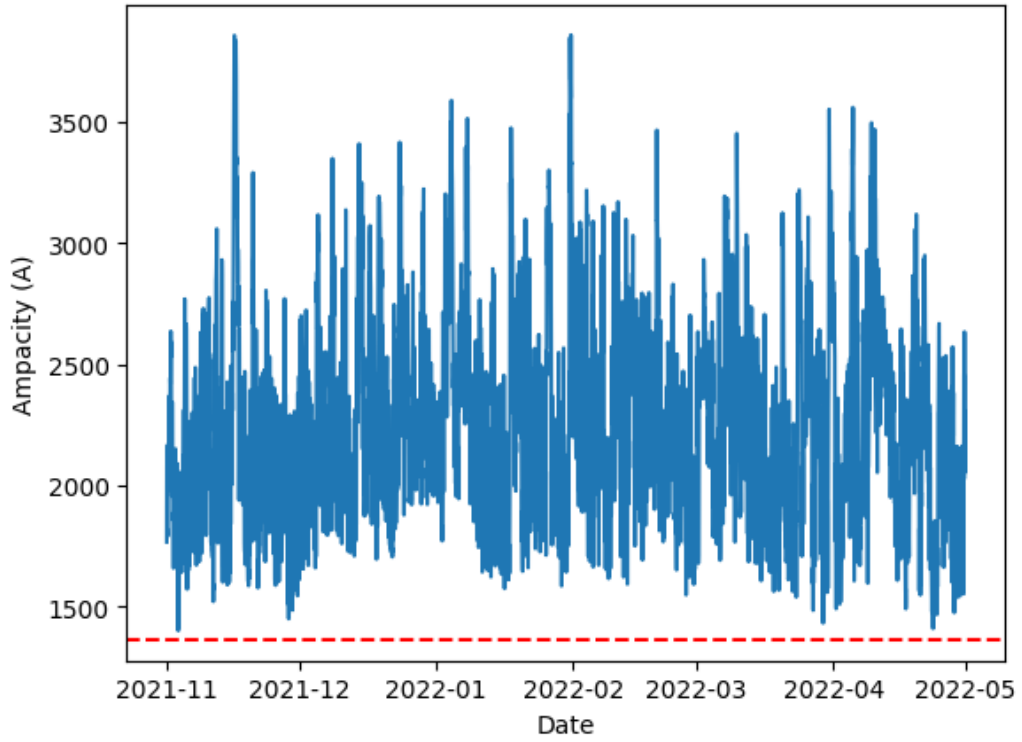
### 4.2.1 Dynamic thermal line rating calculation

DTLR was calculated for a single Falcon wire conductor following the methodology described in Section 4.1.3. The results are visualized in Fig. 4.4a showing the calculated DTLR values for the six winter months from 2021-11-01 to 2022-04-31, alongside the distribution histograms illustrating the percentage current gain in Fig. 4.4b. The red dotted line represents the SR for reference.

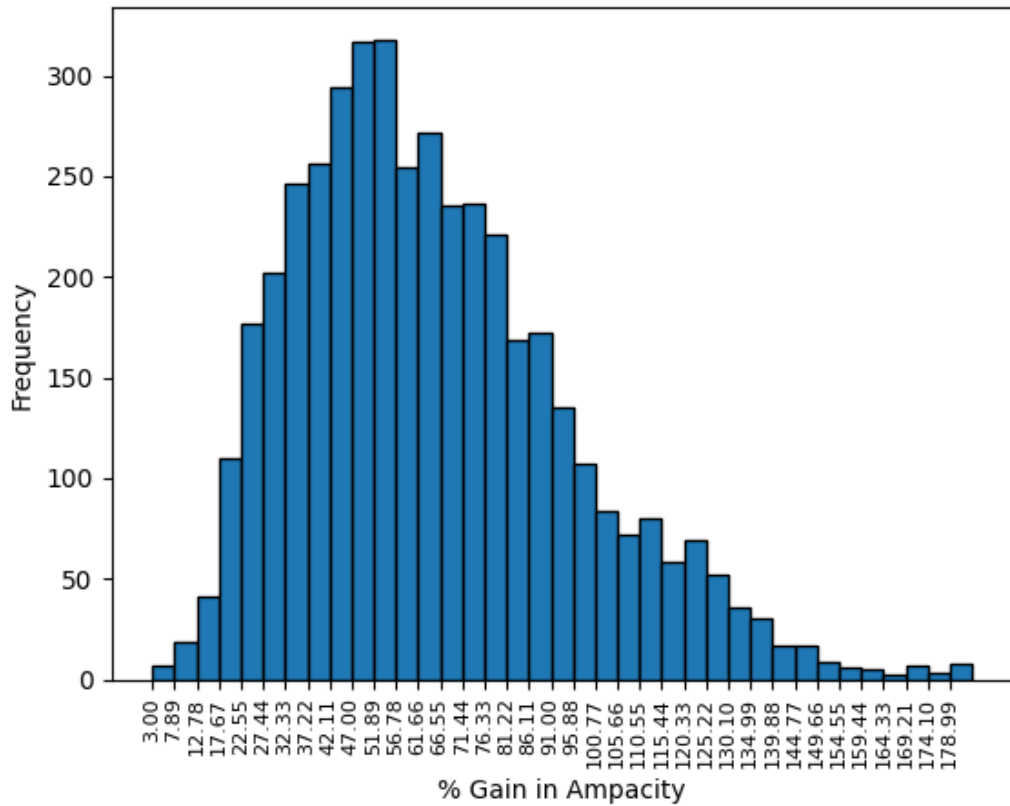
Similarly, Fig. 4.5a shows the calculated hourly DTLR values for the summer period spanning from 2022-05-01 to 2022-10-31 while Fig. 4.5b provides a visual representation of the percentage gain in currents during the summer months.

Analyzing the outcome, the observed average gain in thermal rating for a single conductor across the entire transmission line stands at 883.34 A during the six winter months and 467.83 A throughout the six summer months. These values demonstrate the untapped potential for increased current capacity. They indicate that, in real-time scenarios, the lines are often underutilized, leaving room for enhanced power transfer. Conversely, a loss of 375.78 A in capacity in the summer months is observed under the least favorable conditions. This highlights the possibility of overloading the line under the least favorable conditions with the conservative estimates provided by static line ratings. In terms of power, considering the 4 bundled conductors connected to the 500 kV system, the potential additional power that could be transferred amounts to 1766.68 MW during winter months and 935.64 MW in summer months.

The scatter plots in Fig. 4.6a and Fig. 4.6b were generated by computing the average DTLR for each hour during the winter and summer seasons. These plots provide a picture of how the transmission capacity changes throughout the day depending on the season. The peaks in the plots illustrate the time of the day when the transmission line can effectively transmit higher power due to favorable weather conditions and troughs indicate when the line experiences adverse weather conditions.

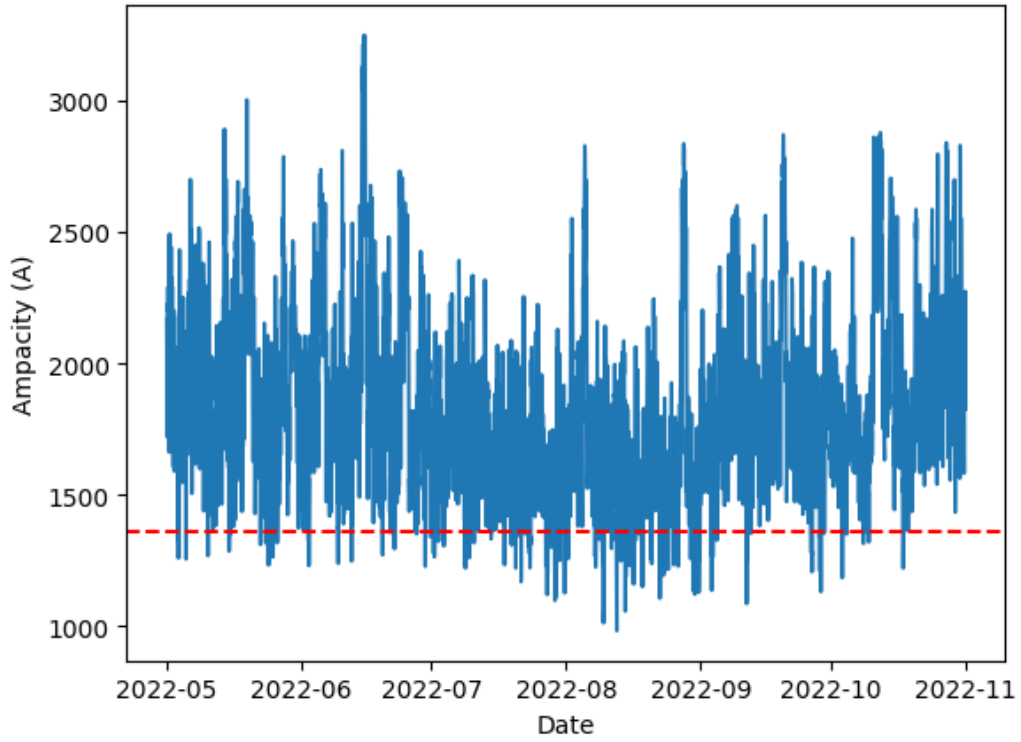


(a) DTLR variation of a single conductor

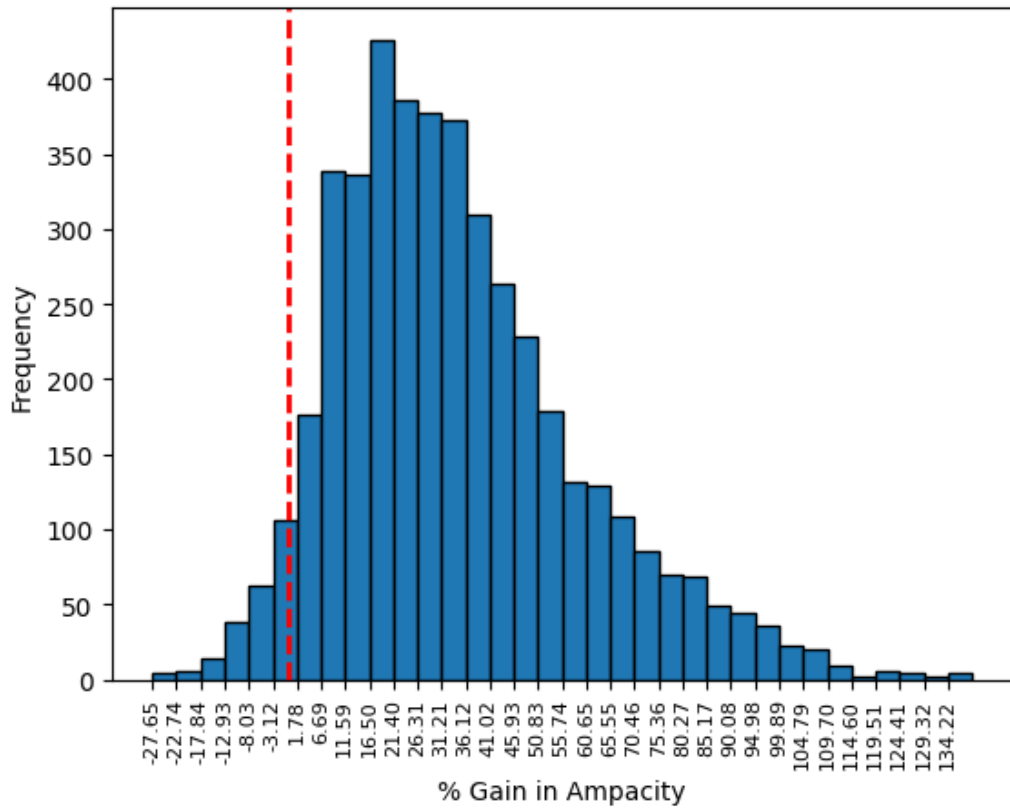


(b) Distribution of percentage gain at a given point of the line

**Figure 4.4:** DTLR variation of the line for six winter months (2021-11-01 to 2022-04-31)

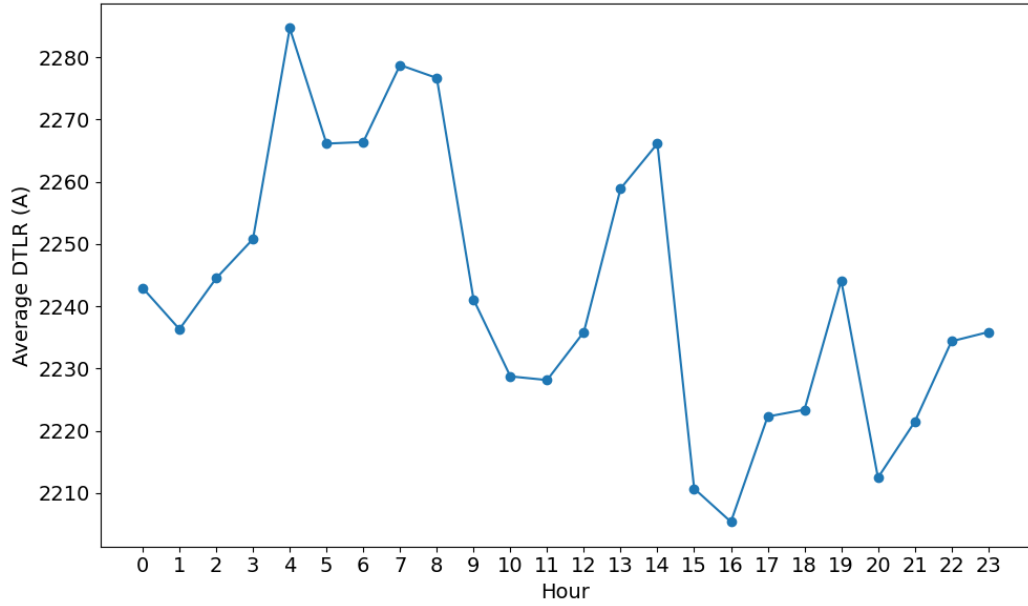


(a) DTLR variation of a single conductor

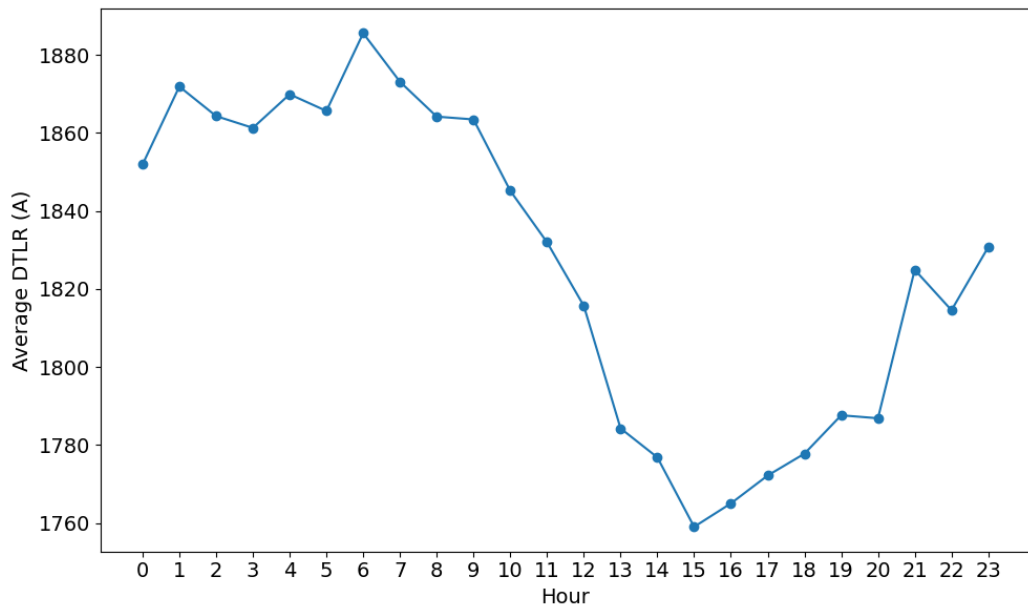


(b) Distribution of percentage gain at a given point of the line

**Figure 4.5:** DTLR variation of the line for six summer months (2022-05-01 to 2022-10-31)



(a) Hourly average DTLR variation throughout a day in winter



(b) Hourly average DTLR variation throughout a day in summer

**Figure 4.6:** Hourly average DTLR variation of a day

## 4.2.2 Wind Power Generation

The performance of a single turbine at JWPP2 was assessed for both winter and summer according to its turbine power curve and weather data. Fig.4.7 illustrates the potential power output from a single turbine during January. According to the calculations, it is evident that a single turbine can generate an average of 2.85 MW of power. Fig.4.8 highlights the variation in the average power output of a turbine throughout the day, with peak generation occurring between 13:00 and 15:00 during a winter month. It suggests that the turbine's performance varies over the day. Furthermore, the total power plant consisting of 13 turbines could supply 37.11 MW to the EATL transmission corridor on average.

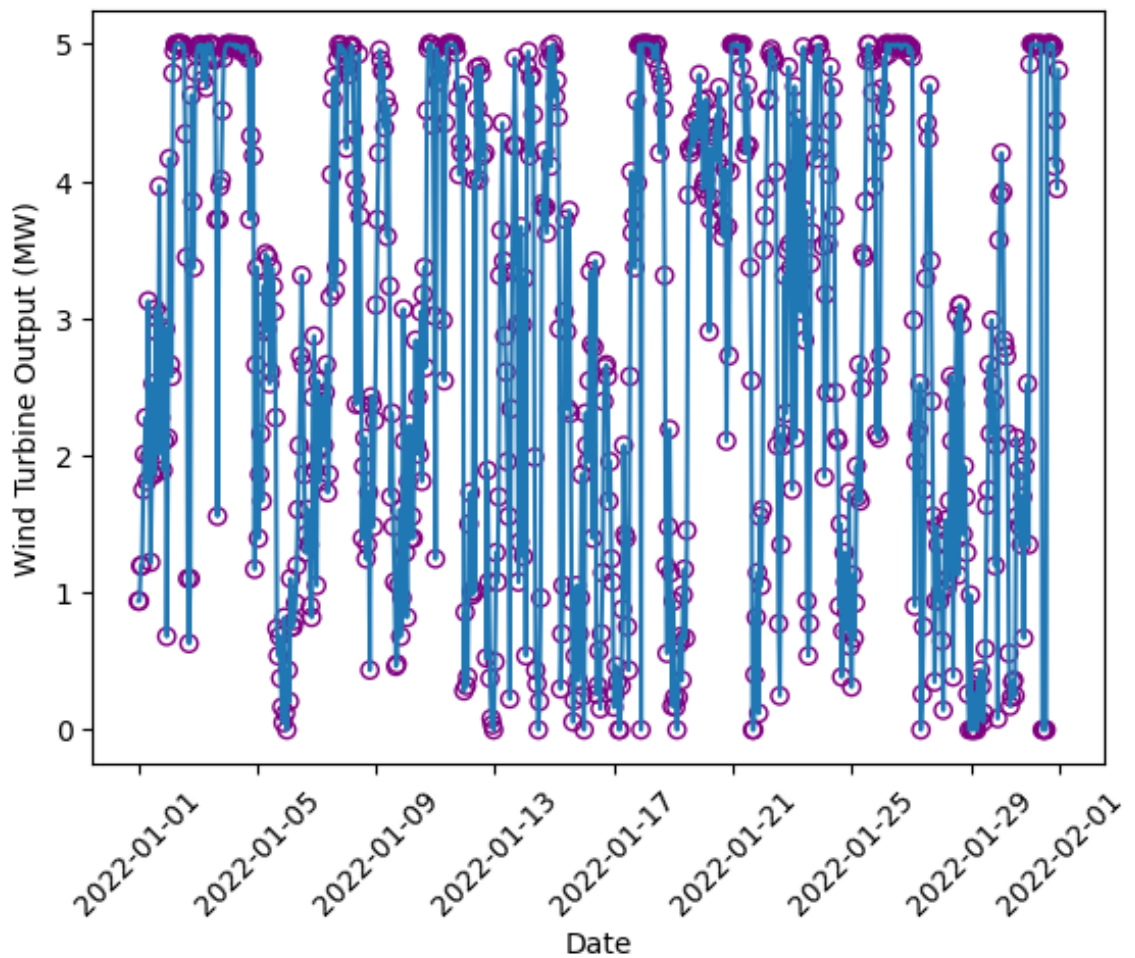


**Figure 4.7:** Power generated by a single turbine at JWPP2 in January

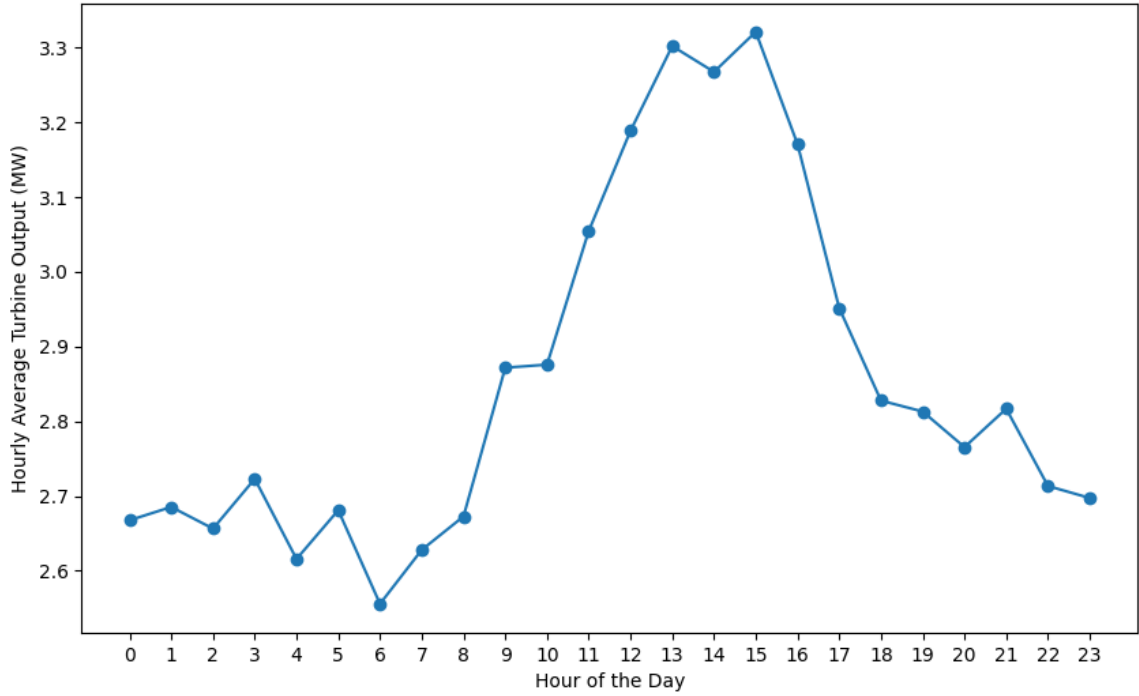


**Figure 4.8:** Average turbine output variation at JWPP2 for a day

### 4.2.3 GHG Reduction

**Table 4.3:** GHG emission reduction by JWPP2 wind plant by using DTLR

Compound	Avg. (T/hr) from JWPP2
Carbon Dioxide	13.78
Sulphur Dioxide	0.10
Nitrogen Oxides	0.067
Methane	15.79
Mercury	$1.51 \times 10^{-8}$

As illustrated by the key pollutants from coal-fired power plants listed in Table 3.2, the emission reductions were calculated for the scenario detailed in Section 4.2.2. Therefore, considering the situation where the transmission line is fully utilized and the additional demand is supplied from the wind energy generated from the wind plant JWPP2 using DTLR, the average reduction of GHG emissions is calculated as presented in Table 4.3. These figures highlight the potential pollution reductions

when coal-fired power plants are replaced with renewable energy sources, utilizing DTLR.

According to the Canada Energy Regulator [105], Alberta’s GHG emissions soared to 256.4 MT of carbon dioxide equivalent ( $CO_2e$ ) in 2020 which has marked a 19% surge since 2005. Additionally, the electricity sector played a crucial role, generating 29.3 MT ( $CO_2e$ )—52% of the total Canadian GHG emissions from power generation. This underscores the ongoing need for sustainable practices to address and mitigate the environmental impact in Alberta. By providing tangible evidence of the positive impact that a single plant with 13 - 5MW wind turbines utilizing DTLR can reduce the  $CO_2$  emissions by 13.7 T/hr, this study highlights a practical and achievable solution to mitigate pollution.

### 4.3 Discussion

Integration of DTLR into HVDC transmission systems is of significant importance for several reasons. As illustrated in Fig.4.4a and Fig.4.5a, the significant fluctuations in DTLR reveal the dynamic interaction with time. In general, the winter months exhibit a greater increase in current carrying capacity above the SR. In contrast, there are some instances during the summer when the DTLR is lower than the SR. This is due to the elevated ambient temperatures in summer, which lead to higher line temperatures, causing reduced line capacity. In contrast, during winter, lower ambient temperatures allow for more heat dissipation from the line, allowing for higher dynamic ratings. The influence of wind is crucial in DTLR by allowing more convective cooling during high wind conditions, potentially improving the capacity of the line. This might explain the variations in line ratings over the day or year.

According to the results described in Section 4.2.1, on average, the line rating can increase from its nominal value up to 64% during winter and 34% during summer. Consequently, the total line gains an additional capacity of 1766.68 MW during winter and 935.66 MW during summer. However, since the focus of this study is on an

HVDC transmission line, it would not be possible to use all of the capacity provided by the DTLR in all cases. The maximum additional capacity that can be used would be limited by the overloading capability of the connected equipment, especially the converters. On a positive note, as noted in the examples described in Chapter 2, the overloading capability of HVDC systems is already being leveraged commercially. This presents an opportunity for HVDC transmission operators to use the advantages of DTLR to meet increasing demand and contribute to reducing GHG emissions.

Assuming a conservative 5% overload for converters for a brief period, considering the examples in Chapter 2, still gives 100 MW additional capacity which can be used during peak demand hours during the day. As demonstrated by the case study in Section 4.2.1, the excess capacity provided by DTLR is more than enough to compensate for the 100 MW allowed. However, more studies are needed to investigate the overloading capability of the HVDC converters. Such exploration will enable the strategic utilization of the total excess transmission capacity provided by DTLR.

According to wind power generation calculations, on average, JWPP2 independently contributes 37.11 MW to the line (with the current configuration of 13 turbines). Additionally, the fluctuations in DTLR over 24 hours, as illustrated in Fig. 4.6a, correlate with changing ambient conditions throughout the day. This provides valuable insights when the DTLR is higher and when it is lower. By aligning these fluctuations with wind power generation patterns (c.f. Fig. 4.8) more renewable energy can be optimally dispatched to the grid without any curtailment. This strategic approach, based on DTLR indications of higher capacity, enables more efficient integration of renewable energy.

Furthermore, from the turbine power output graph in Fig. 4.7, it is evident that the average power generated by a single turbine is less than its rated capacity. The average output slightly surpasses 50% of its nominal rating. This underutilization allows developers to construct much larger wind plants and utilities to connect them to the existing network. Furthermore, in this case study, it has been found that it

would take 35 Enercon E-147 turbines to generate power equal to the excess 100 MW achieved by DTLR. This represents a significant contribution to the reduction of greenhouse gas emissions and underscores the potential to scale up wind power projects to maximize their environmental impact.

# Chapter 5

## Economic Analysis

### 5.1 Introduction

Among many benefits provided by the DTLR from different perspectives, the following are some financial benefits that can be gained directly or indirectly for the utility and consumer.

1. DTLR allows the transmission system operators to monitor the real-time rating of the line, avoiding the curtailment of the most cost-effective power such as hydro. This will allow the consumers to have cheaper electricity with fewer outage times. This will also avoid the unnecessary re-dispatches which will potentially compromise the reliability [106, 107].
2. Maximizing the utilization of the existing infrastructure which will then lead to a higher return on investments for the system operators[106, 107].
3. Sudden or unexpected limitations that can occur in the network can be managed without opting for system upgrades which is not necessary at that moment[106, 107].
4. Wind power owners will get better prices in terms of connection fees and this will reduce the requirement of special protection schemes. This will encourage investors to move towards environmentally friendly generating options[106, 107].

Even though much research has been carried out on different topics related to DTLR, few studies focus on quantifying the economic benefits of applying DTLR. A systematic approach was presented by Chu in [108] on selecting the best possible line from multiple candidate lines to implement DTLR in a way that gives the maximum financial benefit by comparing the fuel cost savings. According to a scheme that has been implemented by the UK's Scottish Power Energy Networks, it is found that deploying DTLR in the system allows a 10% savings in expenses compared to that with required network upgrades [109]. Sanna et al. in [110] presented a methodology to evaluate the economic benefits when DTLR is applied to a transmission network that is suffering from congestion because of thermal limitations. Saiful et al. [106] conducted a quantitative comparison of the economic benefits of applying DTLR for enhancing power transfer through a transmission line compared to other transmission line upgrading methods.

This section of the study provides a comparison of the financial benefits of two scenarios: (1) applying DTLR to the existing transmission line, and (2) upgrading the transmission line capacity by replacing the existing conductor with a higher-capacity conductor. The annual revenues are calculated and compared with each other to understand the optimal option in terms of revenues.

## **5.2 Scenario (1): Applying DTLR to the existing transmission line**

This section will evaluate the revenue that could be generated by applying DTLR on the existing transmission line to enhance the transmission capacity without going for any other infrastructure upgrading methods. In this evaluation, first, the amount of transmitted energy for a year was calculated as:

$$E = P(t) \times t \tag{5.1}$$

where  $P(t)$  is the amount of electrical power transmitted and  $t$  is the time period.

The DTLR value considered in this annual energy assessment was selected based on the average DTLR value from the whole year. In this study, the value of the DTLR of each hour was calculated for 12 months starting from 2021-11-01 to 2022-10-31 utilizing hourly weather data. Since the study was originally divided into summer and winter periods, the averages for each period were taken into account and the annual average was calculated giving a rating of 2034.86 A per single conductor. Using this rating, the allowed energy flow ( $E_{DLR}$ ) during an hour for the entire year was calculated.

Therefore, the energy flow for the whole year considering DTLR is:

$$\begin{aligned}
 E_{DTLR} &= P(t) \times t \\
 &= 4 \times V \times I_{DTLR} \times t \\
 &= 4 \times 500 \times 10^3 \times 2034.86 \times 365 \\
 &= 1485.45 \text{ GWh/year}
 \end{aligned} \tag{5.2}$$

Similarly, considering the static rating of the line, which is 1359 A in this case for a single ACSR Falcon wire, the amount of energy that could be transferred throughout the whole year can be calculated as:

$$\begin{aligned}
 E_{SR} &= P(t) \times t \\
 &= 4 \times V \times I_{SR} \times t \\
 &= 4 \times 500 \times 10^3 \times 1359 \times 365 \\
 &= 992.07 \text{ GWh/year}
 \end{aligned} \tag{5.3}$$

As observed from the results, it can be seen that the amount of allowable energy transmitted is significantly increased with the DTLR ( $\sim 150\%$ ). The theoretical amount of energy that could be transferred from the DTLR is around 1.5 times when compared to the amount of energy transmitted from only considering the static

rating. Hence, if the demand increases, there will be no curtailments or load shedding if the DTLR is employed. Calculating the additional amount of energy allowable to transmit through the DTLR;

$$\begin{aligned}
 \Delta E_{DTLR} &= E_{DTLR} - E_{SR} \\
 &= 1485.45 - 992.07 \\
 &= 493.38 \text{ GWh/year}
 \end{aligned} \tag{5.4}$$

Moreover, when implementing DTLR on transmission lines, there are some costs incurred with the implementation. One of the main features of implementing DTLR would be to have efficient communication and monitoring techniques available. Indirect monitoring methods such as weather parameter monitoring from weather stations would be simpler yet the accuracy is sometimes compromised. Therefore, in this evaluation, a CAT-1 dynamic line rating system is considered installed in the line.

The one-time product cost of single tower CAT-1 instrumentation (2 load cells, one in each direction) is considered as USD 33,000 [111] for a single conductor (installation, shipment, and operation and maintenance costs are not included in this). It is assumed that the CAT-1 device is connected to the 4-bundled conductors at each tension tower along the EATL line. The EATL consists of 1387 towers in total. It is further assumed that no more than 30% of the towers are tension towers [112]. Hence, the net annual income ( $I_{annual}$ ) on the additionally allowed energy flow through the transmission line can be expressed as [106]:

$$I_{annual} = \Delta E_{DTLR} \times \lambda - D_e \tag{5.5}$$

where  $\lambda$  represents the electricity price in \$/kWh and  $D_e$  is the expenditure. The monthly electricity prices given for Encor by EPCOR [113] given in Table 5.1, are considered and the average value for a year is calculated for use by  $\lambda$ .

Substituting the discovered values into eq. 5.5 ( US\$1  $\approx$  CA\$ 1.34 ):

**Table 5.1:** Encor’s electricity price history in Alberta from 2021-11-01 to 2022-10-31

Month	Electricity Price (¢/kWh)
November 2021	10.572
December 2021	14.105
January 2022	10.332
February 2022	11.601
March 2022	7.962
April 2022	12.138
May 2022	12.465
June 2022	13.847
July 2022	16.853
August 2022	31.498
September 2022	29.842
October 2022	15.343
Average	15.55

$$\begin{aligned}
I_{annual} &= 493.38 \times 10^6 \times \frac{15.55}{100} - 1387 \times 33,000 \times 30\% \times 1.34 \\
&= CA\$ 58.32 \text{ M/year}
\end{aligned} \tag{5.6}$$

The financial benefit gained from employing DTLR cannot be simply divided between the stakeholders i.e. wind power producers, utility, transmission, or distribution system operators due to its dynamic nature. Furthermore, due to the complexity of the engagement of different stakeholders, allocating income or benefits has also become a complex process. Therefore, the economic benefit is assessed by considering the advantage of the rise in power throughout the line [106].

$$\begin{aligned}
\frac{I_{annual}}{\Delta E_{DTLR}} &= \frac{58.32}{493.38} \\
&= CA\$ 0.12 \text{ M/GWh}
\end{aligned} \tag{5.7}$$

It can be seen that for a 1 GWh increment in transmittable energy through the line, there will be a CA\$ 0.12 M financial benefit when DTLR is employed.

### 5.3 Scenario (2): Upgrading transmission line conductor size

In this scenario, the revenue made by replacing the existing transmission line conductors with an appropriate higher rating conductor is considered to enhance the energy flow through the transmission line. The existing conductor is an ACSR Falcon wire conductor with a rating of 1359 A. The conductors are assumed to be replaced with the Bluebird conductor which has a rating of 1623 A to extend the power transfer capability.

Once the existing conductors are replaced by the new conductors, it is obvious that the amount of energy that could be transferred via the line is increased due to its higher static rating. Therefore, the amount of energy that could be transferred due to the upgrading can be calculated as:

$$\begin{aligned}
 E_u &= 4 \times V \times I_{SR} \times t \\
 &= 4 \times 500 \times 10^3 \times 1623 \times 365 \\
 &= 1184.79 \text{ GWh/year}
 \end{aligned} \tag{5.8}$$

Further, due to the increase in energy flow, the additional amount of energy compared to the previous conductor which had a lower rating than the new conductor can be calculated as:

$$\begin{aligned}
 \Delta E_u &= E_{SR,new} - E_{SR,before} \\
 &= 1184.79 - 992.07 \\
 &= 192.72 \text{ GWh/year}
 \end{aligned} \tag{5.9}$$

When it comes to cost, the main portion comes with the capital cost incurred for

buying a new conductor. The capital cost to replace the 4-bundled conductor of the 485 km long line is taken to be US\$ 251.43 M. Therefore,

$$\begin{aligned} C_{u,t} &= 1.34 \times 251.43 \times 10^6 \\ &= CA\$ 336.92 \text{ M} \end{aligned} \quad (5.10)$$

As most infrastructure development projects are financed with loans, it is assumed the same for this case with a 7.02% nominal interest rate ( $r$ ) and a 30-year payback period ( $n$ ). Therefore, the annuity method is incorporated to assess the annual capital cost ( $C_{u,a}$ ) of upgrading the conductor. First, the annuity ( $a$ ) is calculated as in the below equation [114]:

$$\begin{aligned} a &= \frac{r \times (1 + r)^n}{(1 + r)^n - 1} \\ &= \frac{0.0702 \times (1 + 0.0702)^{20}}{(1 + 0.0702)^{20} - 1} \\ &= 0.08 \end{aligned} \quad (5.11)$$

Once the annuity is calculated, the annual capital cost for replacing the conductor is calculated.

$$\begin{aligned} C_{u,a} &= a \times C_{u,t} \\ &= 0.08 \times 336.92 \times 10^6 \\ &= CA\$ 26.95 \text{ M/year} \end{aligned} \quad (5.12)$$

Similar to scenario 1, the annual revenue can be calculated using the equation 5.13:

$$\begin{aligned} I_{u,a} &= \Delta E_u \times \lambda - C_{u,a} \\ &= 192.72 \times 10^6 \times \frac{15.55}{100} - 26.95 \times 10^6 \\ &= CA\$ 3.01 \text{ M/year} \end{aligned} \quad (5.13)$$

Further, the benefit of upgrading the conductor with a new conductor is calculated as:

$$\begin{aligned}\frac{I_{u,a}}{\Delta E_u} &= \frac{3.01}{192.72} \\ &= \text{CA\$ } 0.02 \text{ M/GWh}\end{aligned}\tag{5.14}$$

It is observed that for a 1 GWh increment in transmittable energy through the line when the line goes through a conductor upgrade, there will be a CA\$ 0.02 M financial benefit.

## 5.4 Financial benefit comparison

In this section, two scenarios were considered to compare the financial benefits in CA\$ M/ GWh of each method. Results achieved for using DTLR to enhance the capacity of the transmission corridors and upgrading the existing conductors with a higher rating are illustrated in Table 5.2.

**Table 5.2:** Financial benefit comparison

Capacity enhancing method	Benefit (CA\$ M / GWh)
Using DTLR	0.12
Conductor rating upgrading	0.02

When comparing the calculated results, it is shown that using DTLR for capacity enhancement yields a benefit that is 83.33% greater than the benefit obtained from conductor upgrading according to the assumptions that were taken into account. Hence, using DTLR for capacity upgrading has significantly higher benefits in comparison to upgrading the conductors. Even though conventional methods such as upgrading conductors or construction of new transmission lines are typically the most popular solutions for enhancing the transmission corridor capacities, innovative solutions such as utilizing the DTLR would justify the economical benefits over the conventional methods.

Further, not only the financial benefits but also some qualitative benefits which are achievable are demonstrated in Table 5.3.

**Table 5.3:** Qualitative benefit comparison

Qualitative Benefit	Using DTLR	Conductor rating upgrading
Power disruptions	low	high
Service downtime	low	high
Reliability	low	high
Longevity	low	high

The economic benefits such as revenues gained from replacing the conductors can be quantified more accurately because the factors influencing the revenues such as the amount of energy transfer can be quantified due to known information. Nevertheless, when it comes to dynamic rating, the revenues cannot be predicted accurately due to the variations in factors affecting the revenue.

# Chapter 6

## Conclusions & Future Work

### 6.1 Conclusions

This thesis conducts a dynamic thermal line rating study for an LCC-based  $\pm 500$  kV overhead bipolar HVDC transmission line, EATL, located in Alberta, Canada. Real-world line and meteorological parameters are adopted to develop a practical case study system that accounts for typical summer and winter (seasonal) conditions. The key conclusions of this work are summarized below:

1. Accounting for the DTLR aspect of the HVDC transmission line results in a mean ampacity increase of 64% during winter and 34% during summer as compared to using the classical SR of the HVDC conductors. The relatively lower DTLR rating during the summer months is due to elevated ambient temperatures, which lead to higher line temperatures, yielding a lower overall potential increase in the line's current carrying capacity. During the winter months, the lower ambient temperatures and higher wind availability permit more heat dissipation from the line and consequently a higher DTLR. These results underscore the potential to increase utilization of the existing HVDC transmission corridor, particularly during seasonal peaks in demand, without any up-front capital investment.
2. In this study, the additional transmission capacity achieved through DTLR

yields an average potential reduction of 13.78 T/hr in  $CO_2$  by power production of just 13 E-147 turbines. This highlights the potential opportunity to connect larger wind plants, or, more broadly speaking, the potential to inject more power generated by renewable sources into the HVDC transmission corridor. By doing so, pollutant-emitting coal-fired power plants can be replaced by cleaner and sustainable energy sources that offer reduced GHG emissions.

3. Comparing the financial benefits in this study, using DTLR for power flow capacity enhancement yields an 83.33% greater benefit when compared to traditional conductor upgrading. Even though conventional methods such as upgrading conductors or construction of new transmission lines have historically been the most popular solutions for enhancing the transmission corridor capacities, innovative solutions such as utilizing the DTLR can be far more cost-effective. Moreover, little effort is needed to implement DTLR while it can take years to construct new lines when accounting for the necessary regulatory approvals.
4. The realization of full power flow capacity offered by DTLR in larger HVDC networks is somewhat restricted due to limitations of the overloading capability of the power electronic converters at each end of the line. This is due to the relatively tight thermal time constants of the semiconductor switches. However, as the LCC-based HVDC technology considered in this thesis is known to provide higher overload capability (both short and long term) relative to VSC-based technology, this work gives merit to the idea of temporary but strategic overloading of LCC stations in order to fully utilize the maximum possible benefits of DTLR. Although more research is needed, the case study system developed in this thesis provides a solid foundation for such investigations.

## 6.2 Future Work

While this thesis has focused on implementing dynamic thermal line rating for HVDC transmission corridors to mitigate GHG emissions, there are further investigations that can be carried out to have a better understanding of the real-time operating conditions in the context of HVDC transmission.

1. Short-term and long-term overloading of the converters in HVDC transmission corridors can be further investigated when the line is operating at its thermal rating.
2. Simulation models can be developed to better understand how the voltage, currents, etc. at the AC and DC sides of the HVDC stations change when DTLR is applied.
3. The study can be extended to consider multi-terminal HVDC transmission networks to understand how to optimally allocate the DTLR of each transmission line and what would be the correct time to allocate the DTLR.
4. A study can be carried out to understand the reliability of applying the DTLR technique in HVDC transmission corridors. For example, how the DTLR affects the aging of conductors, converters, and other transmission equipment.

# Bibliography

- [1] P. Kacejko, M. Wydra, W. Nowak, W. Szpyra, and R. Tarko, “Advantages, benefits, and effectiveness resulting from the application of the dynamic management of transmission line capacities,” in *2018 15th International Conference on the European Energy Market (EEM)*, 2018, pp. 1–5. DOI: 10.1109/EEM.2018.8469777.
- [2] W. Bao, Y. Yan, W. Zhang, J. Xin, Z. Li, and R. Tang, “Field study of a novel dynamic rating system for power transmission lines,” in *2015 5th International Conference on Electric Utility Deregulation and Restructuring and Power Technologies (DRPT)*, 2015, pp. 1726–1731. DOI: 10.1109/DRPT.2015.7432512.
- [3] H. R. Rajaram and G. Balamurugan, “A study on green house gas mitigation from solar parks in india,” in *2020 International Conference and Utility Exhibition on Energy, Environment and Climate Change (ICUE)*, 2020, pp. 1–8. DOI: 10.1109/ICUE49301.2020.9307039.
- [4] S. D. Foss, S. H. Lin, and R. A. Fernandes, “Dynamic thermal line ratings part i dynamic ampacity rating algorithm,” *IEEE Transactions on Power Apparatus and Systems*, vol. PAS-102, no. 6, pp. 1858–1864, 1983. DOI: 10.1109/TPAS.1983.317795.
- [5] B. P. Bhattarai *et al.*, “Improvement of transmission line ampacity utilization by weather-based dynamic line rating,” *IEEE Transactions on Power Delivery*, vol. 33, no. 4, pp. 1853–1863, 2018. DOI: 10.1109/TPWRD.2018.2798411.
- [6] J. Engelhardt and S. Basu, “Design, installation, and field experience with an overhead transmission dynamic line rating system,” in *Proceedings of 1996 Transmission and Distribution Conference and Exposition*, 1996, pp. 366–370. DOI: 10.1109/TDC.1996.545961.
- [7] L. Rácz and B. Németh, “Dynamic line rating—an effective method to increase the safety of power lines,” *Applied Sciences*, vol. 11, no. 2, 2021, ISSN: 2076-3417. DOI: 10.3390/app11020492.
- [8] E. Fernandez, I. Albizu, G. Buigues, V. Valverde, A. Etxegarai, and J. G. Olazarri, “Dynamic line rating forecasting based on numerical weather prediction,” in *2015 IEEE Eindhoven PowerTech*, 2015, pp. 1–6. DOI: 10.1109/PTC.2015.7232611.

- [9] J. Fu, D. J. Morrow, S. Abdelkader, and B. Fox, "Impact of dynamic line rating on power systems," in *2011 46th International Universities' Power Engineering Conference (UPEC)*, 2011, pp. 1–5.
- [10] D. Balangó, I. Pácsónyi, and B. Németh, "Overview of a new dynamic line rating system, from modelling to measurement," in *2015 5th International Youth Conference on Energy (IYCE)*, 2015, pp. 1–6. DOI: 10.1109/IYCE.2015.7180801.
- [11] U. D. of Energy. "Dynamic line ratings for transmission lines – topical report." Accessed on November, 2023. (2014), [Online]. Available: [https://www.energy.gov/sites/prod/files/2016/10/f34/SGDP\\_Transmission\\_DLR\\_Topical\\_Report\\_04-25-14.pdf](https://www.energy.gov/sites/prod/files/2016/10/f34/SGDP_Transmission_DLR_Topical_Report_04-25-14.pdf).
- [12] R. Puffer, M. Schmale, B. Rusek, C. Neumann, and M. Scheufen, "Area-wide dynamic line ratings based on weather measurements," in *Proceedings of the Conference on Cigre Session*, vol. 44, 2012.
- [13] S. Abdelkader, D. Morrow, J. Fu, and S. Abbot, "Field measurement based pls model for dynamic rating of overhead lines in wind intensive areas," *Renewable Energy and Power Quality Journal*, pp. 808–813, Mar. 2013. DOI: 10.24084/repqj11.454.
- [14] D. V. Hertem, O. Gomis-Bellmunt, and J. Liang, "Lcc-hvdc systems," in *HVDC Grids - For Offshore and Supergrid of the Future*, John Wiley & Sons, 2016, ch. 3.2.
- [15] CIGRE WG B2.42, "Guide for thermal rating calculations of overhead lines," CIGRE, Paris, Tech. Rep. Technical Brochure 601, 2014.
- [16] A. Michiorri *et al.*, "Forecasting for dynamic line rating," *Renewable and Sustainable Energy Reviews*, vol. 52, pp. 1713–1730, 2015, ISSN: 1364-0321. DOI: <https://doi.org/10.1016/j.rser.2015.07.134>. [Online]. Available: <https://www.sciencedirect.com/science/article/pii/S1364032115007819>.
- [17] V. Morgan, "Rating of bare overhead conductors for continuous currents," English, *Proceedings of the Institution of Electrical Engineers*, vol. 114, 1473–1482(9), 10 Oct. 1967, ISSN: 0020-3270.
- [18] H. E. House and P. D. Tuttle, "Current-carrying capacity of acsr," *Transactions of the American Institute of Electrical Engineers. Part III: Power Apparatus and Systems*, vol. 77, no. 3, pp. 1169–1173, 1958. DOI: 10.1109/AIEEPAS.1958.4500119.
- [19] "Ieee standard for calculating the current-temperature relationship of bare overhead conductors," *IEEE Std 738-2012 (Revision of IEEE Std 738-2006 - Incorporates IEEE Std 738-2012 Cor 1-2013)*, pp. 1–72, 2013. DOI: 10.1109/IEEESTD.2013.6692858.

- [20] M. Davis, “A new thermal rating approach: The real time thermal rating system for strategic overhead conductor transmission lines – part i: General description and justification of the real time thermal rating system,” *IEEE Transactions on Power Apparatus and Systems*, vol. 96, no. 3, pp. 803–809, 1977. DOI: 10.1109/T-PAS.1977.32393.
- [21] TWENTIES project, *Final report*, 2013.
- [22] F. Qiu and J. Wang, “Distributionally robust congestion management with dynamic line ratings,” *IEEE Transactions on Power Systems*, vol. 30, no. 4, pp. 2198–2199, 2015. DOI: 10.1109/TPWRS.2014.2361012.
- [23] M. Mahmoudian Esfahani and G. R. Yousefi, “Real time congestion management in power systems considering quasi-dynamic thermal rating and congestion clearing time,” *IEEE Transactions on Industrial Informatics*, vol. 12, no. 2, pp. 745–754, 2016. DOI: 10.1109/TII.2016.2530402.
- [24] J. Vinklers, N. Chokani, and R. S. Abhari, “Improved integration of european renewables using dynamic line rating in switzerland,” in *2016 13th International Conference on the European Energy Market (EEM)*, 2016, pp. 1–5. DOI: 10.1109/EEM.2016.7521236.
- [25] T. Yip, C. An, G. Lloyd, M. Aten, and B. Ferri, “Dynamic line rating protection for wind farm connections,” in *2009 CIGRE/IEEE PES Joint Symposium Integration of Wide-Scale Renewable Resources Into the Power Delivery System*, 2009, pp. 1–5.
- [26] E. Cloet and J.-L. Lilien, “Uprating transmission lines through the use of an innovative real-time monitoring system,” in *2011 IEEE PES 12th International Conference on Transmission and Distribution Construction, Operation and Live-Line Maintenance (ESMO)*, 2011, pp. 1–6. DOI: 10.1109/TDCLLM.2011.6042218.
- [27] S. D. Kim and M. M. Morcos, “An application of dynamic thermal line rating control system to up-rate the ampacity of overhead transmission lines,” *IEEE Transactions on Power Delivery*, vol. 28, no. 2, pp. 1231–1232, 2013. DOI: 10.1109/TPWRD.2012.2234940.
- [28] World Bank Group, “Smart grid to enhance power transmission in vietnam,” Tech. Rep., 2016.
- [29] A. V. Kabović, M. M. Kabović, S. V. B. Rakas, and V. V. Timčenko, “Short-term wind forecasting based on time series data for dynamic line rating,” in *2017 25th Telecommunication Forum (TELFOR)*, 2017, pp. 1–4. DOI: 10.1109/TELFOR.2017.8249456.
- [30] A. Jiang, Z. Jiang, H. Dai, J. Liu, L. Fu, and L. Tang, “Design and application of dynamic line rating system for distribution lines,” in *2018 China International Conference on Electricity Distribution (CICED)*, 2018, pp. 332–336. DOI: 10.1109/CICED.2018.8592213.

- [31] M. H. A. Aziz, N. S. Miswan, F. A. Mohd.Kasran, M. S. Muhamad Shokri, M. N. Noran, and A. A. Rahim, "Pilot project on dynamic line rating (dlr) system for optimal use of tenaga nasional berhad (tnb) grid capacity," in *2020 International Conference on Technology and Policy in Energy and Electric Power (ICT-PEP)*, 2020, pp. 77–81. DOI: 10.1109/ICT-PEP50916.2020.9249936.
- [32] L. RÁCZ and B. NÉMETH, "A novel concept of dynamic line rating systems based on soft computing models," in *2022 10th International Conference on Smart Grid (icSmartGrid)*, 2022, pp. 131–136. DOI: 10.1109/icSmartGrid55722.2022.9848683.
- [33] I. E. Agency. "World energy outlook 2022." License: CC BY 4.0 (report); CC BY NC SA 4.0 (Annex A), IEA. (2022), [Online]. Available: <https://www.iea.org/reports/world-energy-outlook-2022>.
- [34] I. E. Agency. "World energy outlook 2021," IEA. (2021), [Online]. Available: <https://www.iea.org/reports/world-energy-outlook-2021>.
- [35] J. L. Holechek, H. M. E. Geli, M. N. Sawalhah, and R. Valdez, "A global assessment: Can renewable energy replace fossil fuels by 2050?" *Sustainability*, 2022. [Online]. Available: <https://api.semanticscholar.org/CorpusID:248313260>.
- [36] N. Zhang, H. Li, C. Gao, G. Qiu, J. Chen, and G. Sheng, "Wind farm transmission line capacity increase based on dynamic matching of wind turbine power and line current-carrying characteristics," in *2022 Power System and Green Energy Conference (PSGEC)*, 2022, pp. 380–385. DOI: 10.1109/PSGEC54663.2022.9881022.
- [37] Federal Ministry of Economic Affairs and Climate Action, "Germany's current climate action status," Tech. Rep., Tech. Rep., p. 13.
- [38] North American Reliability Corporation, "2009 long-term reliability assessment," Technical Report, Tech. Rep., Nov. 2009.
- [39] K.-K. Cao, T. Pregger, J. Haas, and H. Lens, "To prevent or promote grid expansion? analyzing the future role of power transmission in the european energy system," *Frontiers in Energy Research*, vol. 8, 2021, ISSN: 2296-598X. DOI: 10.3389/fenrg.2020.541495. [Online]. Available: <https://www.frontiersin.org/articles/10.3389/fenrg.2020.541495>.
- [40] L. Welder *et al.*, "Design and evaluation of hydrogen electricity reconversion pathways in national energy systems using spatially and temporally resolved energy system optimization," *International Journal of Hydrogen Energy*, vol. 44, no. 19, pp. 9594–9607, 2019, Special Issue on Power To Gas and Hydrogen applications to energy systems at different scales - Building, District and National level, ISSN: 0360-3199. DOI: <https://doi.org/10.1016/j.ijhydene.2018.11.194>. [Online]. Available: <https://www.sciencedirect.com/science/article/pii/S0360319918338552>.

- [41] T. Ringelband, M. Lange, M. Dietrich, and H.-J. Haubrich, "Potential of improved wind integration by dynamic thermal rating of overhead lines," in *2009 IEEE Bucharest PowerTech*, 2009, pp. 1–5. DOI: 10.1109/PTC.2009.5281897.
- [42] P. Schell, J. Lambin, B. Godard, H.-M. Nguyen, and J.-L. Lilien, "Using dynamic line rating to minimize curtailment of wind power connected to rural power networks," 2011.
- [43] A. K. Kazerooni, J. Mutale, M. Perry, S. Venkatesan, and D. Morrice, "Dynamic thermal rating application to facilitate wind energy integration," in *2011 IEEE Trondheim PowerTech*, 2011, pp. 1–7. DOI: 10.1109/PTC.2011.6019215.
- [44] S. Talpur, C. J. Wallnerstrom, C. Flood, and P. Hilber, "Implementation of dynamic line rating in a sub-transmission system for wind power integration," *Smart Grid and Renewable Energy*, vol. 6, no. 8, 6401392, pp. 233–249, QC 20150824. DOI: 10.4236/sgre.2015.68020.
- [45] J. Teh and I. Cotton, "Reliability impact of dynamic thermal rating system in wind power integrated network," *IEEE Transactions on Reliability*, vol. 65, no. 2, pp. 1081–1089, 2016. DOI: 10.1109/TR.2015.2495173.
- [46] B. Banerjee, D. Jayaweera, and S. M. Islam, "Optimal scheduling with dynamic line ratings and intermittent wind power," in *2014 IEEE PES General Meeting — Conference & Exposition*, 2014, pp. 1–5. DOI: 10.1109/PESGM.2014.6939381.
- [47] M. Laughton and D. Warne, "Reasons for choosing hvdc," in *Electrical Engineer's Reference Book (16th Edition)*, Elsevier, 2003, ch. 32.2.4.
- [48] A. Millard, "Thomas edison, the battle of the systems and the persistence of direct current," *Material Culture Review*, vol. 36, no. 1, Jun. 1992. [Online]. Available: <https://journals.lib.unb.ca/index.php/MCR/article/view/17509>.
- [49] A. Bayo Salas, "Operation, control and optimization of a meshed-hvdc system," Ph.D. dissertation, UPC, Escola Universitària d'Enginyeria Tècnica Industrial de Barcelona, Jun. 2013.
- [50] G. Asplund, L. Carlsson, and O. Tollerz, "50 years hvdc part ii: The semiconductor 'takeover'," *ABB Review*, pp. 10–13, Jan. 2003.
- [51] Alstom, *H.V.D.C. HVDC for Beginners and Beyond*. Saint-Ouen, France, 2010.
- [52] M. P. Bahrman, "Hvdc transmission overview," in *2008 IEEE/PES Transmission and Distribution Conference and Exposition*, 2008, pp. 1–7. DOI: 10.1109/TDC.2008.4517304.
- [53] H. Ying, L. Chun-hua, and H. Wei-huang, "A novel scheme of refurbishing the existing lcc-hvdc to vsc-hvdc," in *The 16th IET International Conference on AC and DC Power Transmission (ACDC 2020)*, vol. 2020, 2020, pp. 1767–1772. DOI: 10.1049/icp.2020.0361.

- [54] A. Alassi, S. Bañales, O. Ellabban, G. Adam, and C. MacIver, “Hvdc transmission: Technology review, market trends and future outlook,” *Renewable and Sustainable Energy Reviews*, vol. 112, pp. 530–554, 2019, ISSN: 1364-0321. DOI: <https://doi.org/10.1016/j.rser.2019.04.062>.
- [55] “Special report: 60 years of hvdc,” *ABB Technical Journal*, 2011, ISSN: 1013-3119.
- [56] O. E. Oni, I. E. Davidson, and K. N. Mbangula, “A review of lcc-hvdc and vsc-hvdc technologies and applications,” in *2016 IEEE 16th International Conference on Environment and Electrical Engineering (EEEIC)*, 2016, pp. 1–7. DOI: 10.1109/EEEIC.2016.7555677.
- [57] ENTSO-E. “Voltage source converters.” (2023), [Online]. Available: <https://www.entsoe.eu/Technopedia/techsheets/voltage-source-converters>.
- [58] A. STAN, S. Costinas, and G. Ion, “Overview and assessment of hvdc current applications and future trends,” *Energies*, vol. 15, Feb. 2022. DOI: 10.3390/en15031193.
- [59] N. R. Watson and J. D. Watson, “An overview of hvdc technology,” *Energies*, vol. 13, no. 17, 2020, ISSN: 1996-1073. DOI: 10.3390/en13174342.
- [60] V. K. Sood, *HVDC and FACTS Controllers: Applications of Static Converters in Power Systems*. Amsterdam, The Netherlands: Kluwer Academic Publishers, 2004.
- [61] K. Meah and S. Ula, “Comparative evaluation of hvdc and hvac transmission systems,” Jul. 2007, pp. 1–5. DOI: 10.1109/PES.2007.385993.
- [62] A. Ahmuda, “The corona effect on high voltage transmission lines,” vol. 08, pp. 29–31, Dec. 2019.
- [63] A. D. Andersen, “No transition without transmission: Hvdc electricity infrastructure as an enabler for renewable energy?” *Environmental Innovation and Societal Transitions*, vol. 13, pp. 75–95, 2014, ISSN: 2210-4224. DOI: <https://doi.org/10.1016/j.eist.2014.09.004>. [Online]. Available: <https://www.sciencedirect.com/science/article/pii/S2210422414000690>.
- [64] G. Boyle, *Renewable energy : power for a sustainable future*. Oxford University Press in association with the Open University, 2012, ISBN: 0199545332.
- [65] C. Meyer, M. Hoing, A. Peterson, and R. W. De Doncker, “Control and design of dc grids for offshore wind farms,” *IEEE Transactions on Industry Applications*, vol. 43, no. 6, pp. 1475–1482, 2007. DOI: 10.1109/TIA.2007.908182.
- [66] N. Kirby, L. Xu, M. Lockett, and W. Siepmann, “Hvdc transmission for large offshore wind farms,” *Power Engineering Journal*, vol. 16, no. 3, pp. 135–141, 2002. DOI: 10.1049/pe:20020306.
- [67] E. Y. Bitar, R. Rajagopal, P. P. Khargonekar, K. Poolla, and P. Varaiya, “Bringing wind energy to market,” *IEEE Transactions on Power Systems*, vol. 27, no. 3, pp. 1225–1235, 2012. DOI: 10.1109/TPWRS.2012.2183395.

- [68] X. Xiang *et al.*, “Comparison of cost-effective distances for lfac with hvac and hvdc in their connections for offshore and remote onshore wind energy,” *CSEE Journal of Power and Energy Systems*, vol. 7, no. 5, pp. 954–975, 2021. DOI: 10.17775/CSEEJPES.2020.07000.
- [69] M. I. Blanco, “The economics of wind energy,” *Renewable and Sustainable Energy Reviews*, vol. 13, no. 6, pp. 1372–1382, 2009, ISSN: 1364-0321. DOI: <https://doi.org/10.1016/j.rser.2008.09.004>. [Online]. Available: <https://www.sciencedirect.com/science/article/pii/S1364032108001299>.
- [70] L. Xu and B. R. Andersen, “Grid connection of large offshore wind farms using hvdc,” *Wind Energy*, vol. 9, no. 4, pp. 371–382, 2006. DOI: <https://doi.org/10.1002/we.185>. eprint: <https://onlinelibrary.wiley.com/doi/pdf/10.1002/we.185>. [Online]. Available: <https://onlinelibrary.wiley.com/doi/abs/10.1002/we.185>.
- [71] X. Chen *et al.*, “Integrating wind farm to the grid using hybrid multiterminal hvdc technology,” *IEEE Transactions on Industry Applications*, vol. 47, no. 2, pp. 965–972, 2011. DOI: 10.1109/TIA.2010.2102326.
- [72] P. Bresesti, W. L. Kling, R. L. Hendriks, and R. Vailati, “Hvdc connection of offshore wind farms to the transmission system,” *IEEE Transactions on Energy Conversion*, vol. 22, no. 1, pp. 37–43, 2007. DOI: 10.1109/TEC.2006.889624.
- [73] N. B. Negra, J. Todorovic, and T. Ackermann, “Loss evaluation of hvac and hvdc transmission solutions for large offshore wind farms,” *Electric Power Systems Research*, vol. 76, no. 11, pp. 916–927, 2006, ISSN: 0378-7796. DOI: <https://doi.org/10.1016/j.epsr.2005.11.004>. [Online]. Available: <https://www.sciencedirect.com/science/article/pii/S0378779605002609>.
- [74] J. Liang, T. Jing, O. Gomis-Bellmunt, J. Ekanayake, and N. Jenkins, “Operation and control of multiterminal hvdc transmission for offshore wind farms,” *IEEE Transactions on Power Delivery*, vol. 26, no. 4, pp. 2596–2604, 2011. DOI: 10.1109/TPWRD.2011.2152864.
- [75] S. M. Muyeen, R. Takahashi, and J. Tamura, “Operation and control of hvdc-connected offshore wind farm,” *IEEE Transactions on Sustainable Energy*, vol. 1, no. 1, pp. 30–37, 2010. DOI: 10.1109/TSTE.2010.2041561.
- [76] F. D. Bianchi, J. L. Domínguez-García, and O. Gomis-Bellmunt, “Control of multi-terminal hvdc networks towards wind power integration: A review,” *Renewable and Sustainable Energy Reviews*, vol. 55, pp. 1055–1068, 2016, ISSN: 1364-0321. DOI: <https://doi.org/10.1016/j.rser.2015.11.024>. [Online]. Available: <https://www.sciencedirect.com/science/article/pii/S1364032115012769>.
- [77] W. Wang, G. Li, and J. Guo, “Large-scale renewable energy transmission by hvdc: Challenges and proposals,” *Engineering*, vol. 19, pp. 252–267, 2022, ISSN: 2095-8099. DOI: <https://doi.org/10.1016/j.eng.2022.04.017>. [Online]. Available: <https://www.sciencedirect.com/science/article/pii/S2095809922004362>.

- [78] A. Arroyo *et al.*, “Comparison between ieee and cigre thermal behaviour standards and measured temperature on a 132-kv overhead power line,” *Energies*, vol. 8, no. 12, pp. 13 660–13 671, 2015, ISSN: 1996-1073. DOI: 10.3390/en81212391. [Online]. Available: <https://www.mdpi.com/1996-1073/8/12/12391>.
- [79] A. Popelka, D. Jurik, and P. Marvan, “Actual line ampacity rating using pmu,” in *Proceedings of the 21st International Conference on Electricity Distribution (CIRED)*, Frankfurt, Germany, Jun. 2011.
- [80] R. Puffer, M. Schmale, B. Rusek, C. Neumann, and M. Scheufen, “Area-wide dynamic line ratings based on weather measurements,” Jan. 2012.
- [81] A. Michiorri, P. Taylor, S. Jupe, and C. Berry, “Investigation into the influence of environmental conditions on power system ratings,” *Proceedings of The Institution of Mechanical Engineers Part A-journal of Power and Energy - PROC INST MECH ENG A-J POWER*, vol. 223, pp. 743–757, Nov. 2009. DOI: 10.1243/09576509JPE718.
- [82] R. Stephen *et al.*, “Guide for application of direct real-time monitoring systems,” 2012. [Online]. Available: <https://api.semanticscholar.org/CorpusID:107725921>.
- [83] A. Silva and J. Bezerra, “Applicability and limitations of ampacity models for htls conductors,” *Electric Power Systems Research*, vol. 93, pp. 61–66, 2012, ISSN: 0378-7796. DOI: <https://doi.org/10.1016/j.epsr.2012.07.003>. [Online]. Available: <https://www.sciencedirect.com/science/article/pii/S0378779612002039>.
- [84] A. Arroyo *et al.*, “Comparison between ieee and cigre thermal behaviour standards and measured temperature on a 132-kv overhead power line,” *Energies*, vol. 8, pp. 13 660–13 671, Dec. 2015. DOI: 10.3390/en81212391.
- [85] L. Staszewski and W. Rebizant, “The differences between ieee and cigre heat balance concepts for line ampacity considerations,” Jan. 2010, pp. 1–4, ISBN: 978-83-921315-7-1.
- [86] V. Morgan, “The thermal rating of overhead-line conductors part i. the steady-state thermal model,” *Electric Power Systems Research*, vol. 5, no. 2, pp. 119–139, 1982, ISSN: 0378-7796. DOI: [https://doi.org/10.1016/0378-7796\(82\)90033-5](https://doi.org/10.1016/0378-7796(82)90033-5). [Online]. Available: <https://www.sciencedirect.com/science/article/pii/0378779682900335>.
- [87] N. Schmidt, “Comparison between ieee and cigre ampacity standards,” *IEEE Transactions on Power Delivery*, vol. 14, no. 4, pp. 1555–1559, 1999. DOI: 10.1109/61.796253.
- [88] S. Abbott, S. Abdelkader, L. Bryans, and D. Flynn, “Experimental validation and comparison of ieee and cigre dynamic line models,” in *45th International Universities Power Engineering Conference UPEC2010*, 2010, pp. 1–5.

- [89] P. Pytlak, P. Musilek, and J. Doucet, “Using dynamic thermal rating systems to reduce power generation emissions,” in *2011 IEEE Power and Energy Society General Meeting*, 2011, pp. 1–7. DOI: 10.1109/PES.2011.6039401.
- [90] L. Wilbur and M. Martin, *Handbook of Energy Systems Engineering: Production and Utilization* (Wiley Series in Mechanical Engineering Practice). Wiley, 1985, ISBN: 9780471866336. [Online]. Available: <https://books.google.ca/books?id=QHOBQgAACAAJ>.
- [91] T. Ramachandra, D. Subramanian, and N. Joshi, “Wind energy potential assessment in uttara kannada district of karnataka, india,” *Renewable Energy*, vol. 10, no. 4, pp. 585–611, 1997, ISSN: 0960-1481. DOI: [https://doi.org/10.1016/S0960-1481\(96\)00034-1](https://doi.org/10.1016/S0960-1481(96)00034-1). [Online]. Available: <https://www.sciencedirect.com/science/article/pii/S0960148196000341>.
- [92] A. Garcés and R. E. Torres-Olguin, “2 - hvdc transmission for wind energy: A slow-dynamics model,” in *Modeling, Operation, and Analysis of DC Grids*, A. Garcés, Ed., Academic Press, 2021, pp. 13–25, ISBN: 978-0-12-822101-3. DOI: <https://doi.org/10.1016/B978-0-12-822101-3.00007-1>. [Online]. Available: <https://www.sciencedirect.com/science/article/pii/B9780128221013000071>.
- [93] M. De Lellis, R. Reginatto, R. Saraiva, and A. Trofino, “The betz limit applied to airborne wind energy,” *Renewable Energy*, vol. 127, pp. 32–40, 2018, ISSN: 0960-1481. DOI: <https://doi.org/10.1016/j.renene.2018.04.034>. [Online]. Available: <https://www.sciencedirect.com/science/article/pii/S0960148118304427>.
- [94] C. Carrillo, A. Obando Montaña, J. Cidrás, and E. Díaz-Dorado, “Review of power curve modelling for wind turbines,” *Renewable and Sustainable Energy Reviews*, vol. 21, pp. 572–581, 2013, ISSN: 1364-0321. DOI: <https://doi.org/10.1016/j.rser.2013.01.012>. [Online]. Available: <https://www.sciencedirect.com/science/article/pii/S1364032113000439>.
- [95] T. Ramachandra and B. Shruthi, “Wind energy potential mapping in karnataka, india, using gis,” *Energy Conversion and Management*, vol. 46, no. 9, pp. 1561–1578, 2005, ISSN: 0196-8904. DOI: <https://doi.org/10.1016/j.enconman.2004.07.009>. [Online]. Available: <https://www.sciencedirect.com/science/article/pii/S0196890404001979>.
- [96] I. Tizgui, H. Bouzahir, F. E. Guezar, and B. Benaïd, “Wind speed extrapolation and wind power assessment at different heights,” in *2017 International Conference on Electrical and Information Technologies (ICEIT)*, 2017, pp. 1–4. DOI: 10.1109/EITech.2017.8255215.
- [97] G. Gualtieri, “Surface turbulence intensity as a predictor of extrapolated wind resource to the turbine hub height: Method’s test at a mountain site,” *Renewable Energy*, vol. 120, pp. 457–467, 2018, ISSN: 0960-1481. DOI: <https://doi.org/10.1016/j.renene.2018.01.001>. [Online]. Available: <https://www.sciencedirect.com/science/article/pii/S0960148118300016>.

- [98] C. G. Justus and A. Mikhail, “Height variation of wind speed and wind distributions statistics,” *Geophysical Research Letters*, vol. 3, no. 5, pp. 261–264, DOI: <https://doi.org/10.1029/GL003i005p00261>. eprint: <https://agupubs.onlinelibrary.wiley.com/doi/pdf/10.1029/GL003i005p00261>. [Online]. Available: <https://agupubs.onlinelibrary.wiley.com/doi/abs/10.1029/GL003i005p00261>.
- [99] I. Ahmed, M. Rehan, A. Basit, and K.-S. Hong, “Greenhouse gases emission reduction for electric power generation sector by efficient dispatching of thermal plants integrated with renewable systems,” *Scientific Reports*, vol. 12, Jul. 2022. DOI: 10.1038/s41598-022-15983-0.
- [100] A. Tariq. “Comprehensive overview of the hvdc market of north america and europe,” PTR Inc. (Sep. 2022), [Online]. Available: <https://ptr.inc/comprehensive-overview-of-the-hvdc-market-of-north-america-and-europe>.
- [101] A. E. S. Operator, *AESO 2020 Long-term Transmission Plan*, 2020. [Online]. Available: <https://www.aeso.ca/assets/downloads/AESO-2020-Long-termTransmissionPlan-Final.pdf>.
- [102] A. P. A. Bureaur, *Jenner wind project (phase 1, 2, and 3)*. [Online]. Available: <https://majorprojects.alberta.ca/details/Jenner-Wind-Project-Phase-1-2-and-3/4443> (visited on 10/04/2023).
- [103] R. A. for International Development Cooperation - RoAid, *The expansion of the qartli wind farm - a study of opportunity*, Nov. 2019.
- [104] *Alberta climate information service*, (August 2023). [Online]. Available: <https://acis.alberta.ca>.
- [105] *Provincial and territorial energy profiles – alberta*, (January 2024). [Online]. Available: <https://www.cer-rec.gc.ca/en/data-analysis/energy-markets/provincial-territorial-energy-profiles/provincial-territorial-energy-profiles-alberta.html>.
- [106] S. Talpur, C. J. Wallnerström, P. Hilber, and S. N. Saqib, “Implementation of dynamic line rating technique in a 130 kv regional network,” in *17th IEEE International Multi Topic Conference 2014*, 2014, pp. 477–482. DOI: 10.1109/INMIC.2014.7097387.
- [107] K. A. Sandy, “Dynamic line ratings for optimal and reliable power flow: Enhanced power flow for the smart grid,” in *FERC Technical Conference*, The Valley Group, a Nexans company, 2010.
- [108] R. Chu, “On selecting transmission lines for dynamic thermal line rating system implementation,” *IEEE Transactions on Power Systems*, vol. 7, no. 2, pp. 612–619, 1992. DOI: 10.1109/59.141766.
- [109] G. Murphy. “Implementation of real-time thermal ratings,” Scottish Power Energy Networks. (2013), [Online]. Available: [http://www.spenergynetworks.co.uk/pages/dynamic\\_thermal\\_rating.asp](http://www.spenergynetworks.co.uk/pages/dynamic_thermal_rating.asp).

- [110] S. Uski, “Estimation method for dynamic line rating potential and economic benefits,” *International Journal of Electrical Power & Energy Systems*, vol. 65, pp. 76–82, Feb. 2015. DOI: 10.1016/j.ijepes.2014.09.034.
- [111] I. N. Laboratory, “A guide to case studies of grid enhancing technologies,” Idaho National Laboratory, Tech. Rep. INL-MIS-22-69711, Oct. 2022.
- [112] S. bibinitperiod S. E. Networks, “Dynamic line rating cat-1 addendum report,” Tech. Rep.
- [113] EPCOR. “Epcor - historical electricity rates.” Accessed on: 12 14, 2022. (2022), [Online]. Available: <https://www.epcor.com/products-services/encor/electricity-plans-and-rates/Pages/historical-electricity-rates.aspx>.
- [114] T. Wizelius, *Developing Wind Power Projects: Theory and Practice*, 1st. Routledge, 2007. DOI: 10.4324/9781315781396.